

# A naturally monomeric infrared fluorescent protein for protein labeling *in vivo*

Dan Yu<sup>1,2</sup>, Michelle A Baird<sup>3,4</sup>, John R Allen<sup>3,4</sup>, Elizabeth S Howe<sup>3,4</sup>, Matthew P Klassen<sup>2,5,6</sup>, Anna Reade<sup>2</sup>, Kalpana Makhijani<sup>1,2</sup>, Yuanquan Song<sup>2,5,6</sup>, Songmei Liu<sup>2</sup>, Zehra Murthy<sup>2</sup>, Shao-Qing Zhang<sup>1,2,7</sup>, Orion D Weiner<sup>2</sup>, Thomas B Kornberg<sup>2</sup>, Yuh-Nung Jan<sup>2,5,6</sup>, Michael W Davidson<sup>3,4</sup> & Xiaokun Shu<sup>1,2</sup>

**Infrared fluorescent proteins (IFPs) provide an additional color to GFP and its homologs in protein labeling. Drawing on structural analysis of the dimer interface, we identified a bacteriophytochrome in the sequence database that is monomeric in truncated form and engineered it into a naturally monomeric IFP (mIFP). We demonstrate that mIFP correctly labels proteins in live cells, *Drosophila* and zebrafish. It should be useful in molecular, cell and developmental biology.**

GFP and its red homologs are powerful tools for cell and molecular biology<sup>1,2</sup>. Recently, this fluorescent protein (FP) palette has been extended into the infrared region by introduction of bacteriophytochrome (BphP)-derived IFPs (for example, IFP1.4 and iRFP) that autocatalytically incorporate biliverdin (BV) as the chromophore<sup>3–7</sup>. As a protein fusion tag, an FP should be monomeric so as not to perturb the stoichiometry of the protein of interest. However, most BphPs function as multimeric complexes<sup>8–10</sup>; both IFP1.4 and iRFP are derived from dimeric and truncated BphPs ( $\Delta$ BphP denotes truncations including only the PAS and GAF domains). Whereas iRFP is dimeric, in our previous characterization we reported IFP1.4 and its variant IFP2.0 (ref. 11) to be monomeric. However, we have found that IFP1.4 and IFP2.0 both tend to dimerize at high concentration, with dissociation constants of 7.8  $\mu$ M and 3.7  $\mu$ M, respectively (Supplementary Fig. 1). To develop a robust protein tag in the infrared spectrum, we decided to engineer a naturally monomeric IFP: mIFP.

We first identified a monomeric  $\Delta$ BphP that, judging by the biological fitness of the bacteria expressing the full-length protein,

is unlikely to misfold or aggregate in cells<sup>12</sup>. We hypothesized that some of the many BphP sequences in protein sequence databases might be monomeric in the  $\Delta$ BphP form, which is likely to occur if the protein lacks strong hydrophobic interactions at the putative dimer interface. In contrast, in IFP1.4's parent, *Dr*BphP<sup>13</sup>, the dimer interface includes several residues (Fig. 1a): Leu311 appears to play a critical role, as the mutation L311K disrupts the dimer interface<sup>3</sup>. Analysis of ~40 BphP sequences from the NCBI database revealed *Br*BphP (from *Bradyrhizobium*) as a potential candidate, as the residue corresponding to Leu311 in *Dr*BphP is a polar threonine (Fig. 1b). Indeed, size-exclusion chromatography indicated that  $\Delta$ *Br*BphP eluted later than dimeric  $\Delta$ *Dr*BphP and at a time similar to that of the monomeric form of IFP1.4 (Supplementary Fig. 2), suggesting that  $\Delta$ *Br*BphP is a monomer.

We engineered the nonfluorescent  $\Delta$ *Br*BphP into a fluorescent mutant. In brief, we selected several residues (Asp199, Tyr168, Val178 and Asn258) surrounding BV for saturation mutagenesis, which was followed by DNA shuffling<sup>14</sup> and random mutagenesis. The final fluorescent mutant mIFP absorbed maximally at 683 nm (Supplementary Fig. 3), with excitation and emission maxima of 683 and 704 nm, respectively (Fig. 1c), a quantum yield of 8% and an extinction coefficient of 82,000 M<sup>-1</sup> cm<sup>-1</sup> (Supplementary Table 1). We confirmed that mIFP was monomeric at high concentrations (17 and 34  $\mu$ M) (Fig. 1d and Supplementary Fig. 4). It contains 19 mutations (Supplementary Figs. 5 and 6), including 5 near the D-ring of BV that likely limit its rotation, contributing to the engineered fluorescence by increasing radiative decay of the excited state (Fig. 1e). Mutated residues in mIFP, IFP1.4 and iRFP do not overlap and thus might be targeted for further engineering (Supplementary Fig. 7). mIFP was stable in pH 4–10 (Fig. 1f). Its molecular brightness was similar to that of IFP1.4 and iRFP (Supplementary Table 1), and its cellular brightness was similar to that of iRFP and tenfold greater than that of IFP1.4 in live HeLa cells (Fig. 1g,h and Supplementary Fig. 8). mIFP was 6.3 times more photostable than IFP1.4 (Supplementary Fig. 9) but approximately one-fifth as photostable as iRFP in HEK293 cells (Supplementary Table 1). Photobleaching of mIFP was irreversible (Supplementary Fig. 10), suggesting no residual photoisomerization. mIFP was similar to IFP2.0 and iRFP in terms of maturation rate, BV binding kinetics and affinity (Supplementary Figs. 11–13).

To demonstrate mIFP as a protein tag for use in live-cell imaging, we constructed ~30 mIFP fusion proteins, targeting both the N and C termini with an appropriate-length linker (Online Methods). We successfully expressed and imaged the mIFP fusions in cultured cells without addition of the cofactor, which suggests that mIFP

<sup>1</sup>Department of Pharmaceutical Chemistry, University of California, San Francisco, San Francisco, California, USA. <sup>2</sup>Cardiovascular Research Institute, University of California, San Francisco, San Francisco, California, USA. <sup>3</sup>National High Magnetic Field Laboratory, The Florida State University, Tallahassee, Florida, USA.

<sup>4</sup>Department of Biological Science, The Florida State University, Tallahassee, Florida, USA. <sup>5</sup>Department of Physiology, University of California, San Francisco, San Francisco, California, USA. <sup>6</sup>Howard Hughes Medical Institute, University of California, San Francisco, San Francisco, California, USA. <sup>7</sup>Department of Chemistry, University of Pennsylvania, Philadelphia, Pennsylvania, USA. Correspondence should be addressed to X.S. (xiaokun.shu@ucsf.edu).

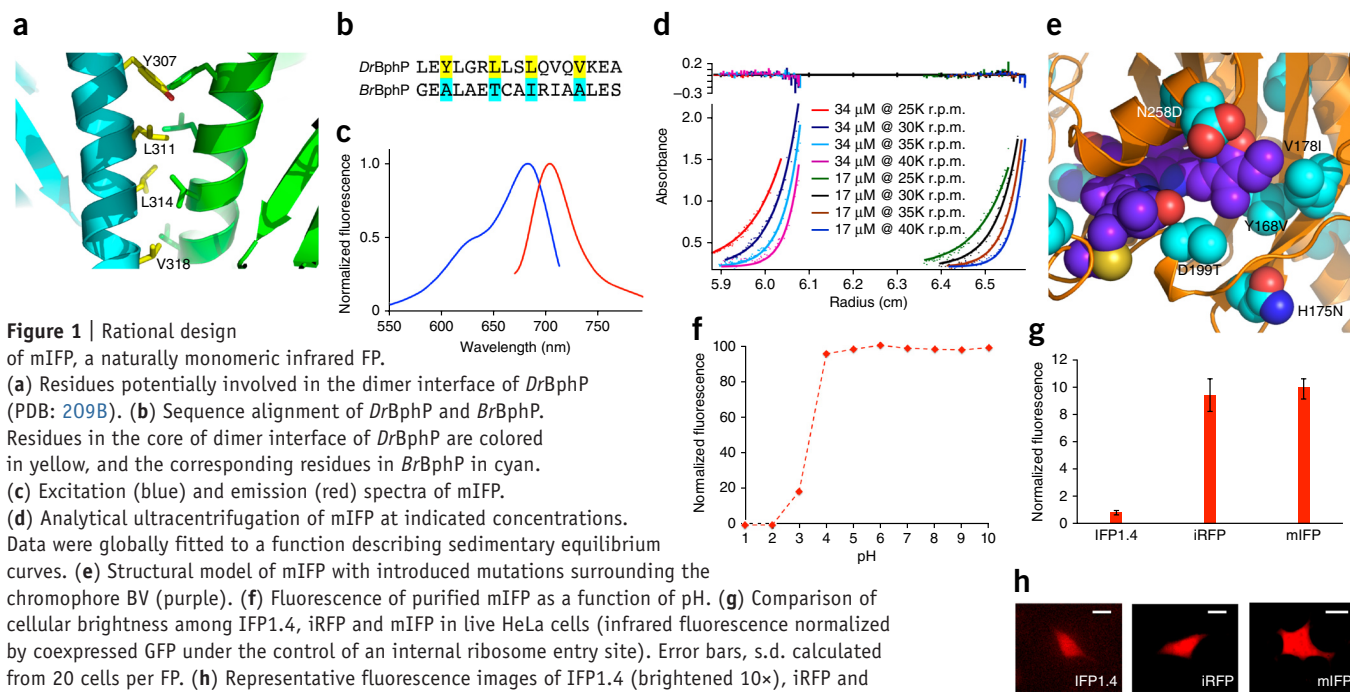


**Figure 1** | Rational design

of mIFP, a naturally monomeric infrared FP.

(a) Residues potentially involved in the dimer interface of DrBphP

(PDB: 209B). (b) Sequence alignment of DrBphP and BrBphP.

Residues in the core of dimer interface of DrBphP are colored

in yellow, and the corresponding residues in BrBphP in cyan.

(c) Excitation (blue) and emission (red) spectra of mIFP.

(d) Analytical ultracentrifugation of mIFP at indicated concentrations.

Data were globally fitted to a function describing sedimentary equilibrium

curves. (e) Structural model of mIFP with introduced mutations surrounding the

chromophore BV (purple). (f) Fluorescence of purified mIFP as a function of pH. (g) Comparison of

cellular brightness among IFP1.4, iRFP and mIFP in live HeLa cells (infrared fluorescence normalized

by coexpressed GFP under the control of an internal ribosome entry site). Error bars, s.d. calculated

from 20 cells per FP. (h) Representative fluorescence images of IFP1.4 (brightened 10 $\times$ ), iRFP and

mIFP in HeLa cells. 20 cells were examined for each FP. Scale bars, 10  $\mu$ m.

used endogenous BV. These fusions localized properly in live cells (Supplementary Figs. 14–16 and Supplementary Videos 1–6), including those that require a high degree of monomeric character, such as  $\alpha$ -tubulin, connexin 43 and intermediate filaments. We observed all phases of mitosis in fusions of mIFP to human histones H1 and H2B. Additionally, mIFP was compatible with structured illumination microscopy (Supplementary Fig. 17).

To demonstrate mIFP as a protein tag in live animals, we created histone fusions and imaged them *in vivo* in fruit flies and zebrafish. For the flies (*Drosophila melanogaster*), we created upstream activating sequence (UAS)-mIFP-histone 3.3 (H3.3) T2A heme oxygenase-1 (HO1) transgenic line and subsequently crossed it with the *engrailed-GAL4* line to promote expression of mIFP-H3.3 in a segmental pattern. Here T2A is a ‘self-cleaving’ peptide widely used in coexpression of multiple genes<sup>15</sup> and HO1 converts heme to BV<sup>16</sup>. Coexpression of this enzyme was necessary to overcome the insufficient levels of endogenous BV in *Drosophila*. Confocal imaging of the embryo detected bright nuclear fluorescence with the expected segmental pattern (Fig. 2a,b). For zebrafish (*Danio rerio*), we expressed mIFP-H2B with HO1 by mRNA injection at the one-cell stage. Imaging of the eye region at 30 hours post fertilization (h.p.f.) revealed bright nuclear fluorescence with the proper expression pattern (Fig. 2c).

To apply mIFP in multicolor labeling *in vivo*, we coexpressed mIFP-H3.3 T2A HO1 and CD8-GFP in neurons of *Drosophila*. CD8 is a transmembrane protein that labels the cell membrane (as is CD4). We observed infrared fluorescence in the nucleus and green fluorescence in the cell membrane in the brain region of embryos, results suggesting correct targeting of the fusion proteins (Fig. 2d–g). We further expressed mIFP T2A HO1 in the abdominal muscle of *Drosophila* larvae, together with a GFP fusion trap of the extracellular matrix protein Viking (collagen) and CD4-tdTomato in class IV dendritic arborization (DA) neurons (ppk::CD4-tdTomato). Fluorescence imaging revealed separation of the three fluorophores (Fig. 2h–j) and the expected structural organization of the labeled

cell types (Fig. 2k). Expression of CD4-mIFP T2A HO1 in class IV DA neurons in *Drosophila* larvae clearly and evenly labeled dendrites and axons (Fig. 2l,m), as expected from previous results with CD4-GFP<sup>17</sup>.

To compare the naturally monomeric mIFP to our previously engineered monomeric IFP2.0 (which was derived from a dimeric parent), we expressed CD4-mIFP T2A HO1 and CD4-IFP2.0 T2A HO1 in epithelial cells of *Drosophila* larvae. Whereas mIFP-CD4 correctly labeled the epithelial cell membrane, IFP2.0-CD4 formed aggregates and failed to label the plasma membrane (Supplementary Fig. 18a,b). This is consistent with *in vitro* data showing that IFP2.0 tends to dimerize at high concentrations.

To demonstrate the use of mIFP in cell labeling, we expressed mIFP in different tissues and compared mIFP to engineered monomeric FPs derived from oligomeric parents, including the popular red FP mCherry, orange FP tdTomato<sup>18</sup> and red FP FusionRed<sup>19</sup> (Supplementary Fig. 18). We found that mCherry formed punctate structures in the muscles and neurons of *Drosophila* first instar larvae. We observed these puncta in the body muscles of each of the more than 200 examined animals. Expression of FusionRed in the leg muscles of adult *Drosophila* revealed many rounded structures, which varied in diameter from 0.5 to 1.3  $\mu$ m; tdTomato formed punctate structures with elongated shape varying in length from 2 to 6  $\mu$ m with width of  $\sim$ 0.4  $\mu$ m. In contrast, mIFP expression was homogeneous in all these contexts, similarly to what we observe with GFP (Supplementary Fig. 19).

To examine potential toxicity of mIFP and HO1, we ubiquitously expressed them in *Drosophila* and conducted a viability assay. We did not find obvious toxicity differences between mIFP or mIFP T2A HO1 and GFP (Supplementary Fig. 20a). Furthermore, we did not observe any defects in the eye morphogenesis of *Drosophila* ubiquitously expressing either mIFP or mIFP T2A HO1, and *Drosophila* embryos expressing mIFP-H3.3 T2A HO1 and CD8-GFP in neurons displayed normal ventral nerve cord shortening without any obvious differences with respect to embryos

**Figure 2** | Expression of mIFP fusions *in vivo*. (a,b) Fluorescence image of *Drosophila* embryo expressing UAS-mIFP-histone 3.3 T2A HO1 driven by *engrailed-GAL4*. (b) High-magnification view of the boxed area in a. (c) Fluorescence image of a zebrafish eye expressing mIFP-H2B and HO1. (d–g) Two-color fluorescence imaging of a *Drosophila* embryo expressing UAS-mIFP-histone 3.3 T2A HO1 and UAS-CD8-GFP, driven by *elav-GAL4*. (d) Whole embryo. (e–g) High-magnification views of the boxed area in d showing GFP expression (e), mIFP expression (f) and a merged image (g). (h–k) Three-color fluorescence imaging of *Drosophila* abdominal muscle expressing UAS-mIFP T2A HO1 driven by *Mef2R-GAL4*, class IV DA neurons expressing CD4-tdTomato (*ppk::CD4-tdTomato*) and extracellular matrix expressing GFP-Viking (collagen): tdTomato (in blue pseudocolor) (h), GFP (i), mIFP (j) and merged (k). (l,m) Class IV DA neurons expressing CD4-mIFP in *Drosophila* larvae. (m) High-magnification view of the boxed area in l. Scale bars: 50  $\mu\text{m}$  (a,d,l), 10  $\mu\text{m}$  (b,e–g) and 20  $\mu\text{m}$  (c,h–k).

expressing CD8-GFP alone (Supplementary Videos 7 and 8). We note that coexpression with HO1 improved mIFP fluorescence by 30- to 40-fold in *Drosophila* muscle (Supplementary Fig. 20b,c). We also observed no obvious toxicity in zebrafish expressing myristoylated mIFP (*myr\_mIFP*) and HO1 by RNA injection at the one-cell stage, evaluated by comparison to zebrafish expressing only GFP (Supplementary Fig. 20d).

To test whether coexpression of HO1 also improves iRFP fluorescence in zebrafish, we expressed myristoylated iRFP (*myr\_iRFP*) with or without HO1 in the tail of embryo at 30 h.p.f. (Supplementary Fig. 21). We observed little iRFP fluorescence in the absence of HO1. Coexpression of HO1 substantially increased iRFP fluorescence, which was obvious in the cell membrane in the tail. Zebrafish expressing *myr\_mIFP* and HO1 showed similar levels of infrared fluorescence in the tail muscle (Supplementary Fig. 21e,f), a finding consistent with our *in vitro* data indicating that mIFP and iRFP have comparable BV binding kinetics and affinity.

In summary, we have engineered a naturally monomeric mIFP that requires biliverdin as a cofactor and have demonstrated its use for protein labeling in living cells and *in vivo*. mIFP is a good template for the development of infrared fluorescent reporters, such as for visualizing cell signaling in live animals. For example, we have designed and recently published an infrared fluorogenic protease reporter based on mIFP that visualizes apoptotic pathways *in vivo*<sup>20</sup>. Protein sequence databases contain thousands of BphPs. These proteins are promising starting points for rational design of future IFPs and related tools with desirable photophysical and photochemical properties.

## METHODS

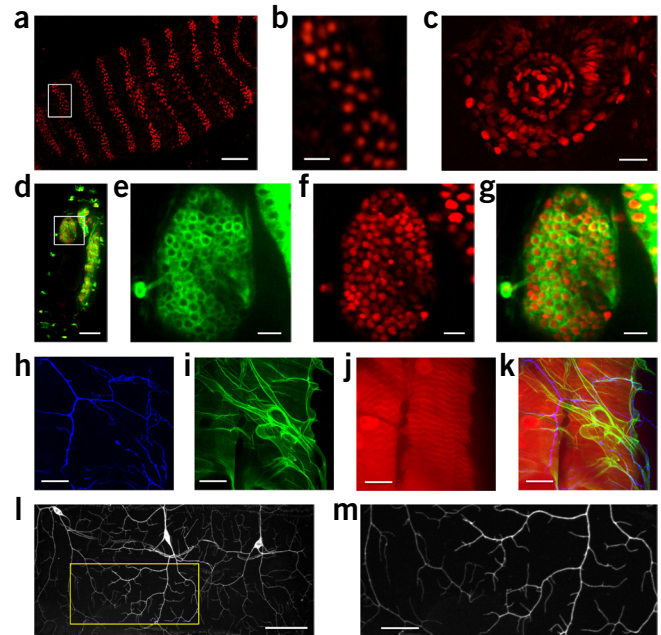
Methods and any associated references are available in the online version of the paper.

**Accession codes.** GenBank/EMBL/DDJB: [KM285236](https://www.ncbi.nlm.nih.gov/nuclot/KM285236).

Note: Any Supplementary Information and Source Data files are available in the online version of the paper.

## ACKNOWLEDGMENTS

This work was supported by the Program for Breakthrough Biomedical Research (to X.S.); US National Institute of Health (NIH) GM030637 (to T.B.K.), GM084040 and GM096164 (to O.D.W.); and the Howard Hughes Medical Institute (to Y.-N.J.). S.-Q.Z. was supported by NIH GM054616 (to W.F. DeGrado) and US National Science Foundation DMR-1120901. We thank N. Joh for assistance in gel filtration chromatography; A. Royant for size-exclusion chromatography; W.F. DeGrado for providing access to the analytical ultracentrifuge;



L.D. Wilsbacher, A. Schepis and S.R. Coughlin for initial testing of mIFP in zebrafish; C.S. Craik for constructive comments; S. Woo at University of California, San Francisco (UCSF) for providing the pCS2+ vector; and S. Roy (UCSF) for providing the UAS-mCherry *Drosophila* line.

## AUTHOR CONTRIBUTIONS

X.S. conceived the project. D.Y. and X.S. designed mIFP and the H2B fusion. K.M. and X.S. planned the *Drosophila* embryo imaging. M.W.D. planned the fusion constructs. T.B.K. planned the histone H3.3 fusion construct and the transgenic *Drosophila*. A.R. and O.D.W. planned the imaging of zebrafish. M.P.K., Y.S. and Y.-N.J. planned the imaging of epithelia, muscle and neurons in *Drosophila* larvae and adults. D.Y., M.A.B., J.R.A., E.S.H., M.P.K., A.R., K.M., Y.S., S.L., Z.M. and S.-Q.Z. performed the experiments. D.Y. and X.S. wrote the manuscript. All the authors contributed to the final draft.

## COMPETING FINANCIAL INTERESTS

The authors declare no competing financial interests.

Reprints and permissions information is available online at <http://www.nature.com/reprints/index.html>.

- Day, R.N. & Davidson, M.W. *Chem. Soc. Rev.* **38**, 2887–2921 (2009).
- Tsien, R.Y. *Angew. Chem. Int. Ed. Engl.* **48**, 5612–5626 (2009).
- Shu, X. *et al. Science* **324**, 804–807 (2009).
- Filonov, G.S. *et al. Nat. Biotechnol.* **29**, 757–761 (2011).
- Auldridge, M.E., Satyshur, K.A., Anstrom, D.M. & Forest, K.T. *J. Biol. Chem.* **287**, 7000–7009 (2012).
- Shcherbakova, D.M. & Verkhusha, V.V. *Nat. Methods* **10**, 751–754 (2013).
- Piatkevich, K.D., Subach, F.V. & Verkhusha, V.V. *Nat. Commun.* **4**, 2153–2162 (2013).
- Giraud, E. & Verméglio, A. *Photosynth. Res.* **97**, 141–153 (2008).
- Rockwell, N.C., Su, Y.S. & Lagarias, J.C. *Annu. Rev. Plant Biol.* **57**, 837–858 (2006).
- Karniol, B., Wagner, J.R., Walker, J.M. & Vierstra, R.D. *Biochem. J.* **392**, 103–116 (2005).
- Yu, D. *et al. Nat. Commun.* **5**, 3626–3632 (2014).
- Geiler-Samerotte, K.A. *et al. Proc. Natl. Acad. Sci. USA* **108**, 680–685 (2011).
- Wagner, J.R., Brunzelle, J.S., Forest, K.T. & Vierstra, R.D. *Nature* **438**, 325–331 (2005).
- Stemmer, W.P. *Nature* **370**, 389–391 (1994).
- Szymczak, A.L. *et al. Nat. Biotechnol.* **22**, 589–594 (2004).
- Cui, L. *et al. Biochem. Biophys. Res. Commun.* **377**, 1156–1161 (2008).
- Han, C., Jan, L.Y. & Jan, Y.-N. *Proc. Natl. Acad. Sci. USA* **108**, 9673–9678 (2011).
- Shaner, N.C. *et al. Nat. Biotechnol.* **22**, 1567–1572 (2004).
- Shemiakina, I.I. *et al. Nat. Commun.* **3**, 1204–1207 (2012).
- To, T.-L. *et al. Proc. Natl. Acad. Sci. USA* **112**, 3338–3343 (2015).

## ONLINE METHODS

**General methods and materials.** A BrBphP gene was ordered from GenScript and cloned into a modified pBAD vector containing the heme oxygenase-1-encoding gene from cyanobacteria. All synthetic DNA oligonucleotides were purchased from Integrated DNA Technologies. Restriction enzymes were purchased from New England BioLabs. Site-specific saturation mutagenesis was performed using a QuickChange Mutagenesis Kit (Stratagene). Random mutagenesis was performed using a GeneMorph II Random Mutagenesis Kit (Stratagene). Libraries were expressed in *Escherichia coli* strain TOP10 (Invitrogen) and screened by imaging the agar plates with colonies using a BioSpectrum Imaging System (UVP). The brightest clone in each library was picked as a template for the next round of random mutagenesis. Cultured cells were not tested for the presence of *Mycoplasma*, as such contamination would not impact the conclusions made on the basis of our imaging results. The sequences of all primers are provided in **Supplementary Table 2**.

**Protein purification and characterization.** mIFP was expressed with a C-terminal polyhistidine tag in a pBAD expression vector (Invitrogen). Proteins were purified with the Ni-NTA purification system (Qiagen). Protein concentration was measured by the Pierce BCA method. Two different approaches were used to determine extinction coefficients. The first one was based on a comparison of absorbance values for the protein at the main peak (683 nm) with the absorbance value at the 391-nm peak, assuming the latter to have the extinction coefficient of the free BV, which is  $39,900 \text{ M}^{-1} \text{ cm}^{-1}$ . The second one was based on direct measurement of the protein concentrations with a BCA protein assay kit (Pierce) followed by the calculation of extinction coefficient using a Beer-Lambert-Bouguer equation. For determination of quantum yield, mIFP solution was prepared with the same absorbance as a solution of Alexa Fluor 647 at wavelength 630 nm (quantum yield = 0.33 in phosphate-buffered saline (PBS)). The absorbance of both solutions is around or below 0.05. Fluorescence from 650 to 800 nm was collected and used to calculate the quantum yield. pH titrations were performed using a buffer series (100 mM sodium acetate, 300 mM NaCl for pH 2.5–5.0 and 100 mM  $\text{NaH}_2\text{PO}_4$ , 300 mM NaCl for pH 4.5–9.0).

To study protein maturation, we grew TOP10 bacterial cells at 37 °C overnight in a LB medium supplemented with ampicillin. The next morning, the cells were centrifuged, resuspended and cultured in LB medium with 0.002% arabinose, 0.001 mM IPTG, 100  $\mu\text{M}$  ALA and 50  $\mu\text{M}$   $\text{FeCl}_3$  for 1 h. The cells were washed and cultured in LB medium supplemented with 0.001 mM IPTG, 100  $\mu\text{M}$  ALA and 50  $\mu\text{M}$   $\text{FeCl}_3$  (no arabinose) at 37 °C. Fluorescence intensity of the cell suspension was measured every hour.

Gel-filtration chromatography was performed using a Superdex-200 HR 10/30 FPLC gel-filtration column (Amersham Biosciences). The column was equilibrated with sterile PBS in a cold room. 100  $\mu\text{l}$  of purified protein at a concentration of 0.5 mg  $\text{ml}^{-1}$  in PBS were loaded in each column. Elution was performed in PBS at a flow rate of 0.5  $\text{ml min}^{-1}$  for 45 min. The column effluent was monitored by absorbance at 280 and 630 nm. The gel-filtration protein standards thyroglobulin, BSA, azurin and aprotinin were also loaded under the same conditions to calibrate the column. The linear calibration curve representing the

logarithm of molecular mass as a function of the fraction number was used to calculate the molecular mass of mIFP.

Analytical ultracentrifugation of mIFP, IFP1.4 and IFP2.0 was carried out by equilibrium sedimentation performed at 25 °C using a Beckman XL-I analytical ultracentrifuge. mIFP solutions were prepared at 34  $\mu\text{M}$  and 17  $\mu\text{M}$ , and IFP1.4 and IFP2.0 solutions were prepared at 17  $\mu\text{M}$  and 8.5  $\mu\text{M}$ , each in a buffer of 50 mM Tris, pH 7.5, 300 mM NaCl, 10 mM imidazole. Centrifugation was conducted at speeds of 25K, 30K, 35K and 40K r.p.m. with an An-60 Ti rotor (**Fig. 1d**), and the radial gradient profiles were acquired by absorbance scans at 280 nm. Data were globally fitted to equilibrium sedimentation models of a single-species and/or monomer-dimer mixtures by a nonlinear least-squares method using Igor Pro (WaveMetrics).

**Fusion plasmid construction.** The mIFP mammalian expression vectors were constructed from C1 or N1 cloning vectors (Clontech-style). The mIFP cDNA was PCR amplified with a 5' primer encoding an AgeI site and a 3' primer encoding either a BspEI (C1) or NotI (N1) site, in reference to mIFP. To prepare the additional 14-amino-acid linker (GGGSGGGSGGGSSG) used for the C-terminal mIFP fusions, we used two primers: mIFP12-AgeI-C-f and mIFP12-BspEI-C-r (**Supplementary Table 2**). The PCR products were gel purified, digested and ligated into EGFP-C1 or EGFP-N1 cloning vectors, respectively, resulting in mIFP C1 and N1 cloning vectors.

To construct the mIFP C-terminal fusions (number of linker amino acids in parenthesis), we performed the following digests: human  $\beta$ -actin (30), NheI and BglII (cDNA source: Clontech; NM\_001101.3); CAF1 (22), AgeI and BspEI (mouse chromatin assembly factor; cDNA source: A. Gunjan, Florida State University; NM\_013733.3); human light chain clathrin (27), NheI and BglII (cDNA source: G. Patterson, NIH; NM\_001834.2); human endosomes (26), NheI and BspEI (human RhoB GTPase; cDNA source: Clontech; NM\_004040.2); human fibrillarlin (19), AgeI and BspEI (cDNA source: Evrogen; NM\_001436.3); H2B (10), BglII and NheI (human histone 2B, cDNA source: G. Patterson, NIH; NM\_021058.3); human lamin A/C (30), NheI and BglII (cDNA source: D. Gilbert, Florida State University; NM\_170707.2); human lasp1 (22) NheI and BglII (cDNA source: OriGene; NM\_006148.3); human myotilin (26), AgeI and BspEI (cDNA source: OriGene; NM\_006790.2); human Rab4a (19), BglII and BamHI (cDNA source: V. Allen, University of Manchester; NM\_004578.3); rat sEpsin (30) NheI and BglII (cDNA source: OriGene; NM\_019585.3); human  $\alpha$ -tubulin (30), NheI and BglII (cDNA source: Clontech; NM\_006082); human vinculin (35) NheI and EcoRI (cDNA source: OriGene; NM\_003373.3).

To prepare the mIFP N-terminal fusions (number of linker amino acids in parenthesis), we performed the following digests: human calnexin (14), AgeI and NotI (cDNA source: OriGene; NM\_001746.3); human CENP-B (22), BamHI and NotI (A. Khodjakov, Wadsworth Center; NM\_001810.5); Cx43 (7), BamHI and NotI (rat  $\alpha$ -1 connexin 43 cDNA source: M. Falk, Lehigh University; NM\_001004099.1); human EB3 (7), BglII and BamHI (cDNA source: L. Cassimeris, Lehigh University; NM\_012326.2); H1 (10), BamHI and NotI (mouse histone 1, cDNA source: G. Patterson, NIH; NM\_008197.3); H2B (6), BamHI and NotI (human histone 2B, cDNA source: G. Patterson,

NIH; NM\_021058.3); human keratin 18 (17), EcoRI and NotI (cDNA source: Open Biosystems; NM\_199187.1); rat lysosomal membrane glycoprotein 1 (20), BamHI and NotI (LAMP1; cDNA source: G. Patterson, NIH; NM\_012857.1); Lifeact (7), BamHI and NotI (cDNA source: Integrated DNA Technologies); human MAPTau (10), AgeI and NotI (cDNA source: OriGene; NM\_016841.4); human nucleoporin 50 kDa (10), BamHI and NotI (NUP50; cDNA source: OriGene; NM\_007172.3); human peroxisomal membrane protein (10), NotI and AgeI (PMP; cDNA source: OriGene; NM\_018663.1); human translocase outer mitochondria membrane 20 (10), (TOMM-20; cDNA source: OriGene; NM\_014765.2); human zyxin (6), BamHI and NotI (cDNA source: OriGene; NM\_003461.4).

DNA for transfection was prepared using the Plasmid Maxi kit (Qiagen).

In summary, the protein of interest can be fused to either the N or C terminus of mIFP. But it is necessary to note that in contrast to N-terminal mIFP fusions, C-terminal fusions often require an extended amino acid linker (see above). On the basis of the crystal structure of an mIFP homolog, the N terminus (first 17 amino acids) is unstructured and forms a flexible loop, whereas the C terminus is highly structured, forming an  $\alpha$ -helix. Limited separation of mIFP and the protein of interest may cause steric hindrance. Inadequate C-terminal linker lengths result in erroneous localization and expression patterns characterized by faint membrane localization and decreased fluorescence. However, optimal linker length must still be determined experimentally.

**Deposition of mIFP fusion plasmid.** The mIFP fusions are available at Addgene. For each fusion, the N- or C-terminal fusion and the linker amino acid length are indicated after the name of the targeted proteins, followed by the Addgene plasmid number: mIFP-N1-54620; mIFP-Calnexin-N-14-56214; mIFP-Endo-14-56219; mIFP-Golgi-7-56221; mIFP-LaminA-C-18-56226; mIFP-Nup50-N-10-56233; mIFP-PMP-N-10-56238; mIFP-Tubulin-C-18-56240; mIFP-Actin-C-18-56211; mIFP-Cx26-7-56216; mIFP-H2B-6-56223; mIFP-Lysosomes-20-56228; mIFP-MapTau-N-10-56230; mIFP-Vimentin-7-56242; mIFP-C-*Src*-7-56213; mIFP-EB3-7-56218; mIFP-ER-5-56220; mIFP-Keratin-17-56225; mIFP-MyosinIIC-N-18-56232; mIFP-PMP-C-10-56237; mIFP-Annexin-12-56212; mIFP-CyTERM-N-17-56217; mIFP-H2B-C-10-56224; mIFP-MANNII-N-10-56229; mIFP-Mito-7-56231; mIFP-PDHA1-N-10-56236; mIFP-Zyxin-6-56243; mIFP-alpha-actinin-19-56210; mIFP-CENPB-N-22-56215; mIFP-H1-10-56222; mIFP-LC-myosin-N-7-56227; mIFP-Paxillin-22-56234; mIFP-Tomm20-N-10-56239; mIFP-VASP-5-56241; mIFP12-C1-54819; mIFP12-Annexin-12-56245; mIFP12-LASP1-C-10-56257; mIFP12-Caveolin-C-10-56247; mIFP12-H2B-C-10-56254; mIFP12-MyosinIIa-C-18-56259; mIFP12-Rab4a-7-56261; mIFP12-Actin-C-18-56244; mIFP12-Clathrin-15-56249; mIFP12-LaminA-C-18-56256; mIFP12-CD81-10-56248; mIFP12-Endo-14-56250; mIFP12-ILK-C-14-56255; mIFP12-sEspin-C-18-56262; mIFP12-CAF1-C-10-56246; mIFP12-FilaminA-C-14-56253; mIFP12-myopalladin-C-14-56258; mIFP12-myotilin-C-14-56260; mIFP12-ZO1-C-14-56265; mIFP12-Fibrillarin-7-56252; mIFP12-Farnesyl-5-56251; mIFP24-C1-54820; mIFP24-Caf1-C-10-56266; mIFP24-LaminA-C-18-56267.

**Characterization and imaging in mammalian cells.** To image mIFP and its fusions in mammalian cells, we transfected HeLa or HEK293 cells with mIFP fusions using the calcium phosphate transfection method, maintained them with regular growth medium (without exogenous BV) and imaged them 48 h after transfection on a Nikon Eclipse Ti inverted microscope equipped with a Yokogawa CSU-W1 confocal scanner unit (Andor), a digital complementary metal-oxide semiconductor (CMOS) camera ORCA-Flash4.0 (Hamamatsu) and an ASI MS-2000 XYZ automated stage (Applied Scientific Instrumentation). Laser inputs were provided by an Integrated Laser Engine (Spectral Applied Research) equipped with laser lines of 405 nm, 488 nm, 561 nm and 640 nm (Coherent). The confocal scanning unit was equipped with the following emission filters: 460/50 nm, 525/50 nm, 610/60 nm, 661/20 nm, 732/60 nm and 731/137 nm. Bright-field and DIC imaging was provided by a Lambda TLED LED transmitted light source (Sutter Instrument). The system was also equipped with a SOLA light engine (Lumencor) for wide-field fluorescence imaging. Images in this study were obtained with the following objectives: Nikon Plan Apo  $\lambda$  20 $\times$  air (numerical aperture (NA), 0.75), Nikon Apo  $\lambda$ S LWD 40 $\times$  water (NA, 1.15), and Nikon Apo TIRF 60 $\times$  oil (NA, 1.49). Image acquisition was controlled by the NIS-Elements Ar Microscope Imaging Software (Nikon). The infrared fluorescence signal of mIFP was excited with the 640-nm laser and collected through the 731/137-nm emitter at 60 $\times$ . All images were processed and analyzed with ImageJ.

Photobleaching of mIFP, iRFP, IFP2.0 or IFP1.4 in live HeLa cells were performed at 60 $\times$ . Cells were excited by the 640-nm laser, and images were taken every 10 s for 30 min and every 1 min afterward.

For studying the dependence of brightness of IFP-expressing cells on BV concentration, LN229 cells stably expressing mIFP, IFP1.4, IFP2.0 or iRFP (each coexpressed with GFP under IRES), grown on 60-mm dishes, were treated with various concentrations of BV for 2 h and collected by centrifugation. The IFP fluorescence was measured using the infinite M1000 plate reader (normalized by coexpressed GFP fluorescence) and was plotted against the BV concentration. s.d. was calculated from 3 independent measurements. To investigate BV binding kinetics, we treated live LN229 cells with 25  $\mu$ M BV. The green and infrared fluorescence intensities were monitored using the infinite M1000 plate reader over time. The infrared fluorescence intensity (normalized by GFP) was plotted against time. s.d. was calculated from 3 independent measurements. To compare the brightness of IFPs in cells by flow cytometer, we transiently transfected live HeLa cells with IFP1.4 IRES EGFP, IFP2.0 IRES EGFP, mIFP IRES EGFP or iRFP IRES EGFP. 48 h after transfection, cells were washed and suspended in 0.5 ml PBS and analyzed on a flow cytometer (FACS Aria III). EGFP fluorescence was detected in the FITC-A channel (488-nm laser, 505- to 535-nm emission filter). IFP fluorescence was detected in the Alexa 700-A channel (640-nm laser, 708- to 753-nm emission filter). Data were processed using FlowJo software.

Structure illumination microscopy (SIM) was performed on a Zeiss Elyra PS.1 super-resolution imaging microscope. Fluorescence was excited using a 642-nm diode laser and 3–5 rotations of the grid pattern, filtered using a 655-nm long-pass filter, and collected using a Zeiss Plan-APOCHROMAT 100 $\times$  (NA, 1.46) oil-immersion objective. All SIM image processing was performed using the proprietary ZEN 2012 Black software (Zeiss).

**Fluorescence imaging in *Drosophila*.** Expression of UAS-mIFP-histone 3.3 was driven by *engrailed-GAL4*. Fluorescence images were taken with the Nikon Eclipse Ti inverted microscope. Transcripts encoding tdTomato, FusionRed, mIFP and mIFP-T2A-HO1 were subcloned into pJFRC81 and phiC31-integrated into the genome at position 75A10 [PBac{y+-attP-9A} VK00005]. UAS::mCherry and UAS::EGFP [P{UAS-2xEGFP}AH2] were previously generated. Expression of these UAS::xFPs was driven ubiquitously [P{tubP-GAL4}LL7, in neurons [P{GMR57C10-GAL4}attP2] or in muscles [P{GAL4-Mef2.R}R1]. For coincident imaging of fluorophores, recombinant flies expressing mIFP-T2A-HO1 in neurons [P{GMR57C10-GAL4}attP2] or muscles [P{GAL4-Mef2.R}R1] were intercrossed to either w[1118], UAS::mCherry, EGFP [P{UAS-2xEGFP}AH2], UAS::tdTomato, UAS::FusionRed. For the triple-labeling experiment, recombinant flies expressing mIFP T2A HO1 in muscles [P{GAL4-Mef2.R}R1] were intercrossed with flies expressing CD4-tdTomato in class IV DA neurons [ppk::CD4-tdTomato] and a GFP fusion trap of the extracellular matrix protein Viking [vkg-PT{G00205}]. Intact first instar larvae were acutely immobilized in water during imaging using a small thermoelectric cooler (Laird) maintained at 4 °C by a PID Relay (Watlow). Condensation arising owing to the temperature differential was mitigated by wiping a thin film of water across the coverslip. Third instar larvae were immobilized in 300 mM sucrose after we removed the distal ends of the cuticle and viscera. Adult female mid-legs were acutely removed and imaged *ex vivo*.

The larval genotypes we used for comparing CD4-mIFP and CD4-IFP2.0 in epithelial cells were w; ppk-CD4-tdGFP/repo-tdTomato; UAS-CD4-mIFP-T2A-H01/A58-Gal4 and w; ppk-CD4-tdGFP/repo-tdTomato; UAS-IFP2.0-T2A-H01/A58-Gal4. Embryos were collected for 2 h on grape juice agar plates treated with yeast and were aged at 25 °C. At the appropriate time, a single larva was mounted in 90% glycerol under coverslips sealed with grease.

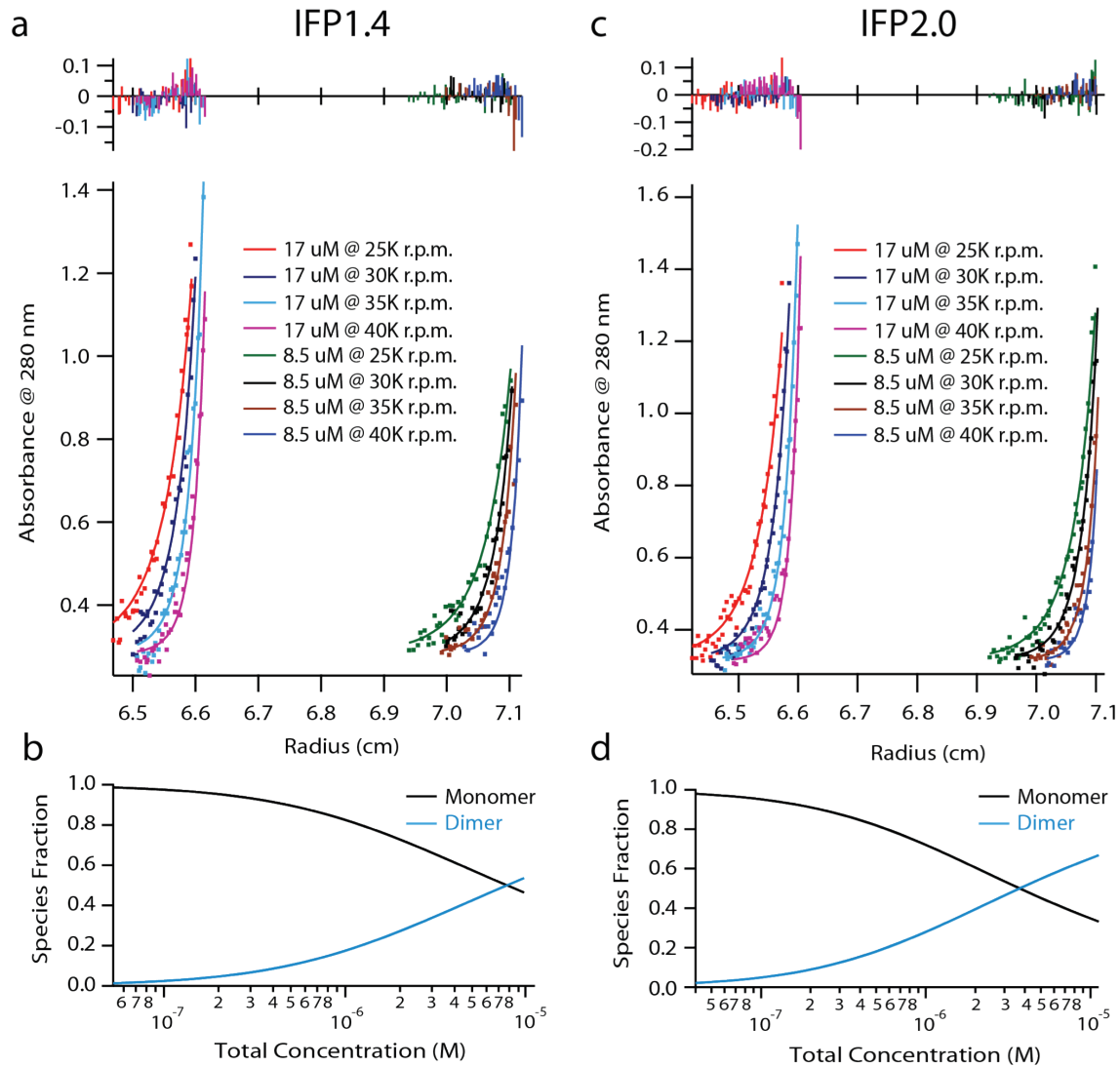
Animals were imaged using the Nikon Eclipse Ti inverted microscope. GFP was imaged with the 488-nm laser and 525/50-nm emission filter at 40 $\times$ , and acquisition time was 100 ms. tdTomato, mCherry and FusionRed were imaged with the 561-nm laser and 610/60-nm emission filter at 40 $\times$ , and acquisition time was 300 ms. IFP2.0 and mIFP were imaged with the 640-nm laser and 731/137-nm emission filter at 40 $\times$ , and acquisition time was

500 ms. Confocal *z* series were acquired using the 20 $\times$  or 40 $\times$  objectives and the digital CMOS camera ORCA-Flash4.0 (Hamamatsu) on the Nikon Eclipse Ti inverted microscope controlled by NIS-Elements Ar Microscope Imaging Software (Nikon).

**Viability assay in *Drosophila*.** Fluorophores were ubiquitously expressed at 25 °C using [P{tubP-GAL4}LL7 or P{w[+mC] = Act5C-GAL4}25FO1], and the adult progeny were examined for eye morphogenesis defects and reduced viability (% of animals carrying the fluorophore transgene relative to a balancer).

**Imaging in zebrafish.** Adult zebrafish, both TL and AB wild-type strains, were maintained under standard laboratory conditions. Expression plasmids pCS2-mIFP-H2B and pCS2-HO1 were created by PCR amplification of mIFP-H2B and HO1 ORFs, respectively, and then cloned into pCS2+. Capped mRNA was synthesized using the mMACHINE SP6 kit (Ambion). 100 pg of mIFP-H2B mRNA with 100 pg of HO1 mRNA were injected at the one-cell stage. Fluorescence and bright-field images were taken at 30 h.p.f. with a charge-coupled device (CCD) camera (Andor; Clara DR-2199) on the Nikon Eclipse Ti microscope. Manually dechorionated embryos were embedded in 1.5% low-melt agarose within glass-bottom Petri dishes (MatTek Corporation). Eye-specific images were taken with a 40 $\times$ /1.3-NA Plan-Fluor oil objective. mIFP fluorescence was imaged with a 638-nm laser line and a red-shifted Cy5.5 filter. *z* stacks of 2.5- $\mu$ m intervals were acquired for each magnification.

**Toxicity assay in zebrafish.** At the one- to two-cell stage, 0, 100, 150 or 200 pg of either Myr-mIFP and HO1 or *gfp* (control) mRNA per embryo were injected. Unfertilized embryos were removed on day 0, and phenotypes of each group were scored alongside uninjected control embryos from the same clutch on day 1 after manual dechorionation. The experiment was performed under constant blue light conditions (465 nm). Each construct had at least *n* = 300 embryos. Embryos were scored as follows: normal to unaffected embryos were considered to have a wild-type phenotype; embryos with the presence of a slightly curved tail and/or mild edema were considered mildly deformed; and embryos with smaller heads, major curves or a kink in the tail and/or severe edema were considered severely deformed.

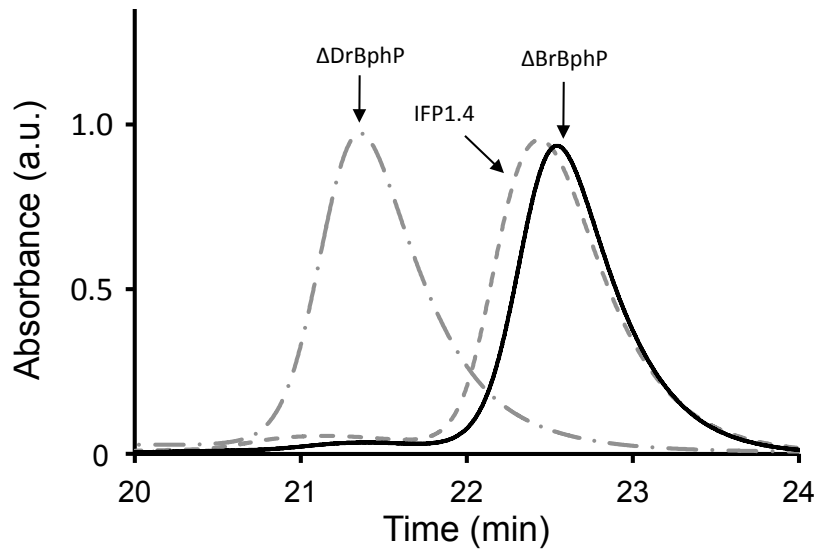


### Supplementary Figure 1

Analytical ultracentrifugation of IFP1.4 and IFP2.0.

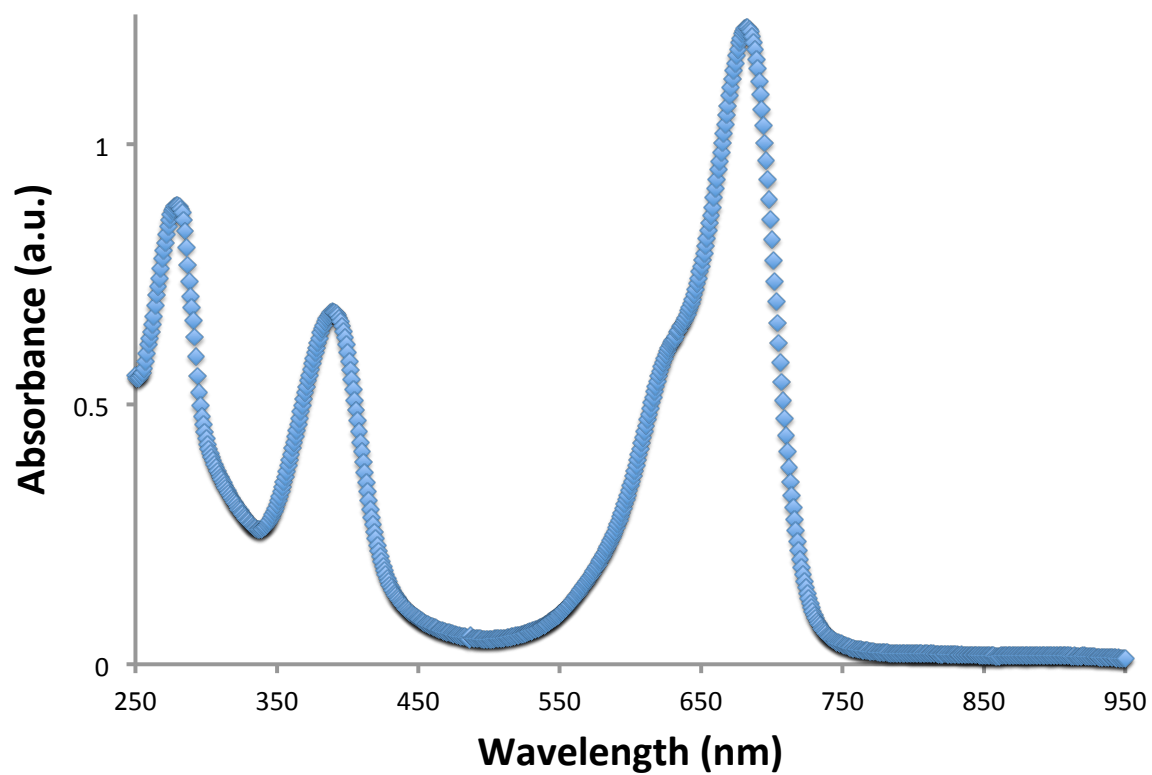
(a) IFP1.4 (molecular weight as 35.909 kD) at 17  $\mu$ M in the buffer 50 mM Tris pH 7.5, 300 mM NaCl, 10 mM Imidazole are centrifuged at four different speeds. Single-species fitting shows that the average molecular weight of IFP1.4 is  $49.323 \pm 3.293$  kD. Global fits as a monomer-dimer equilibrium yield  $K_d$  as  $7.789 \mu$ M (with 95% confidence limits of

4.426 and 13.71  $\mu\text{M}$ ). **(b)** The fractions of the monomer and dimer species of IFP1.4. **(c)** IFP2.0 (molecular weight as 35.952 kD) at 8.5  $\mu\text{M}$  in the buffer 50 mM Tris pH 7.5, 300 mM NaCl, 10 mM Imidazole are centrifuged at four different speeds. Single-species fitting shows that the average molecular weight of IFP2.0 is  $55.237 \pm 2.740$  kD. Global fits as a monomer-dimer equilibrium yield  $K_d$  as 3.722  $\mu\text{M}$  (with 95% confidence limits of 2.186 and 6.337  $\mu\text{M}$ ). **(d)** The fractions of the monomer and dimer species of IFP2.0.



**Supplementary Figure 2.**

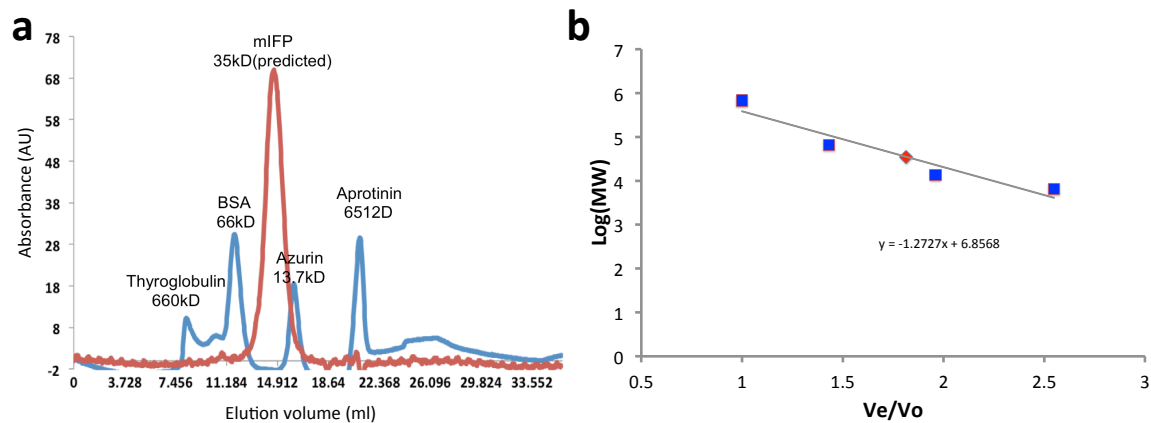
Size exclusion chromatography of  $\Delta BrBphP$ ,  $\Delta DrBphP$  and IFP1.4.



**Supplementary Figure 3.**

Absorbance spectrum of mIFP.

Absorbance of purified mIFP was scanned from 250 to 950 nm every 1nm.



#### Supplementary Figure 4.

Size exclusion chromatography of mIFP.

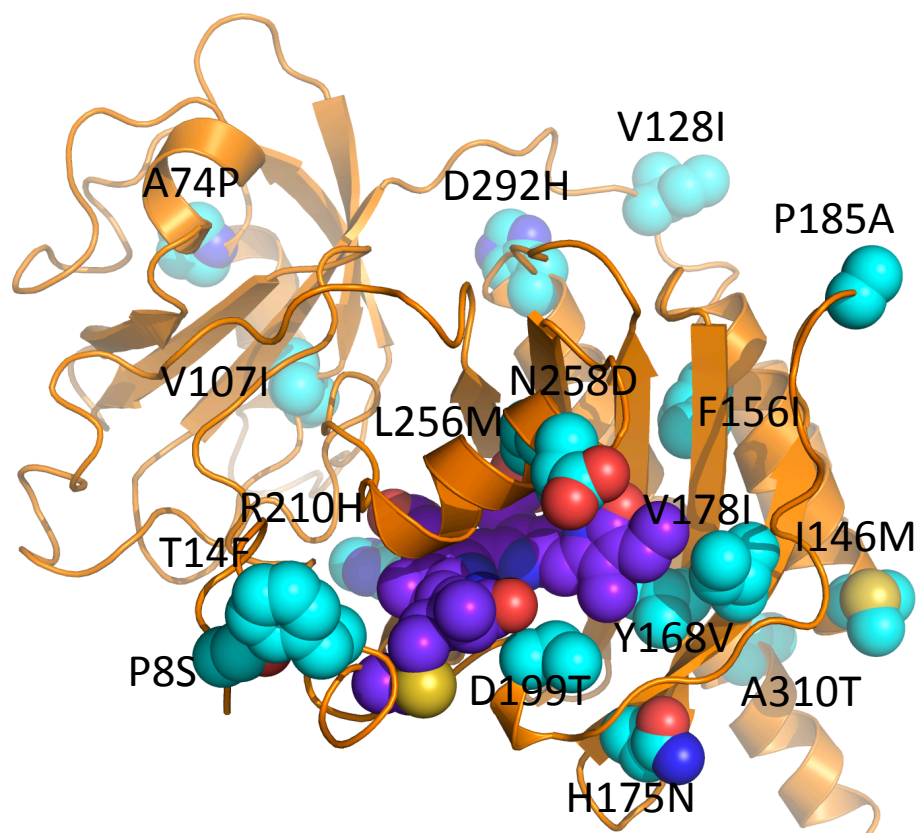
(a) Elution profiles of mIFP. Four standards are also shown: thyroglobulin (669 kDa), BSA (66 kDa), azurin (13.7 kDa), and aprotinin(6512 Da). (b) A standard curve drawn according to peak elution volumes ( $V_e$ , elution volume;  $V_o$ , column volume) for the indicated gel filtration standards as detected by absorption at 280 nm (blue). The estimated position of elution of mIFP was also shown (red). Molecular weight (MW) of mIFP was calculated to be 35.16 kDa from the standard curve, which is close to the theoretical MW of a monomer. The unit of MW in Y-axis is Dalton.

$\Delta$ BrBphP	MPVPLTTPAFGHATLANCEREQIHLAGSIQPHGILLAVKEPDNVVIQASI
mIFP	MSVPLTTS <sup>S</sup> AFGHA <sup>F</sup> LANCEREQIHLAGSIQPHGILLAVKEPDNVVIQASI
$\Delta$ BrBphP	NAAEFLNTNSVVGRLRDLGGDLALQILPHLNGPLHLAPMTLRCTVGSP
mIFP	NAAEFLNTNSVVGRLRDLGGDL <sup>P</sup> LQILPHLNGPLHLAPMTLRCTVGSP
$\Delta$ BrBphP	RRVDCTVHRPSNGGLIVELEPATKTTNVAPALDGAFHRITSSSSLIGLCD
mIFP	RRVDCT <sup>I</sup> HRPSNGGLIVELEPATKTTN <sup>I</sup> APALDGAFHRITSSSSL <sup>M</sup> GLCD
$\Delta$ BrBphP	ETATIFREITGYDRVMVYRFDEEGHGEVLSERRRPDLEAFLGNRYPASDI
mIFP	ETATI <sup>I</sup> REITGYDRVMV <sup>V</sup> RFDEEG <sup>N</sup> GE <sup>I</sup> LSERRR <sup>A</sup> DLEAFLGNRYPAS <sup>T</sup> I
$\Delta$ BrBphP	PQIARRLYERNRVRLLDVNYTPVPLQPRISPLNGRDLDMSSLCLRSMS
mIFP	PQIARRLYE <sup>H</sup> NRVRLLDVNYTPVPLQPRISPLNGRDLDMSSLCLRSMS
$\Delta$ BrBphP	IHQKYLQNMVGATLVCSLMVSGLWGLIACHHYEPRFVFPDIRAAGEAL
mIFP	IHQKY <sup>M</sup> <sup>Q</sup> DMVGATLVCSLMVSGLWGLIACHHYEPRFVFP <sup>H</sup> IRAAGEAL
$\Delta$ BrBphP	AETCAIRIAALESFAQSQSE
mIFP	AETCAIRIA <sup>T</sup> LESFAQSQ <sup>S</sup> <sup>K</sup>

### Supplementary Figure 5.

Sequence alignment between mIFP and its parent  $\Delta$ BrBphP.

The new residues in mIFP are highlighted in yellow.



**Supplementary Figure 6.**

A structural model of mIFP with introduced mutations.

The chromophore BV is shown in purple.

```

ΔDrBphP      MSRDPLPFFPPLYLGGPEITTEHCEREP IHIPGSIQPHGALLTADGHSGEVLQMS-LNAA 59
IFP1.4       MARDPLPFFPPLYLGGPEITTEHCEREP IHIPGSIQPHGALLTADGHSGEVLQVS-LNAA 59
ΔBrBphP      MP---VPLTTPAFG---HATLANCEREQIHLAGSIQPHGILLAVKEPDNVVIQAS-INAA 53
mIFP         MS---VPLTTSAFG---HAFLANCEREQIHLAGSIQPHGILLAVKEPDNVVIQAS-INAA 53
ΔRpBphP      -----MTEGSVAR--QPDLSTCDDEP IHIPGAIQPHGLLLALAADMTIVAGSDNLPEL 51
iRFP         -----MAEGSVAR--QPDLSTCDDEP IHIPGAIQPHGLLLALAADMTIVAGSDNLPEL 51
              :           .           . * : * * * : * : * * * * * * * * : * . :

ΔDrBphP      TFLGQEPTVLRGQTLAALLPEQWPALQAALP-PGCPDALQYRATLDWPAAGHLSLTVHR- 117
IFP1.4       TFLGQEPTVLRGQTLAALLPEQWPALQAALP-PGCPDALQYRATLDWPAAGHLSLTVHR- 117
ΔBrBphP      EFLNTNSVVGR--PLRDLGGDLALQILPHLNGPLHLAPMTLRCTVGSPPR-RVDCTVHRP 110
mIFP         EFLNTNSVVGR--PLRDLGGDLPLQILPHLNGPLHLAPMTLRCTVGSPPR-RVDCTVHRP 110
ΔRpBphP      TGLAIGALIGR-SAADVFDSETHNRLTIALAEPGAAVGAP IAVGFTMRKDAGFVGSWHR- 109
iRFP         TGLAIGALIGR-SAADVFDSETHNRLTIALAEPGAAVGAP IVGFTMRKDAGFVGSWHR- 109
              * . : * . : : : * * . . : : * *

ΔDrBphP      VGELLILEFEP---TEAWDSTGPHALRNAMFALESAPNLRALAEVATQTVRELTFGDRVM 174
IFP1.4       VAELLILEFEP---TEAWDSTGPHALRNAMFALESAPNLRALAEVATQTVRELTFGDRVM 174
ΔBrBphP      SNGGLIVELEP---ATKTTNVAP-ALDGAFHRITSSSSLIGLCDETATIFREITGYDRVM 166
mIFP         SNGGLIVELEP---ATKTTNIAP-ALDGAFHRITSSSSLMGLCDETATIIREITGYDRVM 166
ΔRpBphP      HDQLVFLELEPPQRDVAEPQAFFRRTNSAIRRLQAETLESACAAAQEVREITGFDRVM 169
iRFP         HDQLFLELEPPQRDVAEPQAFFRRTNSAIRRLQAETLESACAAAQEVRITGFDRVM 169
              : : : * * . . . * : : : * . . : : . * : : * * * * *

ΔDrBphP      LYKFAPDATGEVIAEARREGLHAFLGHRFPASDIPAQARALYTRHLLRLTADTRAAAVPL 234
IFP1.4       LYKFAPDATGEMIAEARREGMQAFLGHRFPASHTPAQARALYTRHLLRLTADTRAAAVPL 234
ΔBrBphP      VYRFDEEGHGEVLSERRRPDLEAFLGNRYPASDIPQIARRLYERNRVRLLVDVNYTPVPL 226
mIFP         VVRFDEEGNGEILSERRADEAFLGNRYPASTIPQIARRLYEHNRVRLLVDVNYTPVPL 226
ΔRpBphP      IYRFASDFSGEVIAEDRCAEVESLGLHVPASTVPAQARRLYTINPVRIIPDINYPVPV 229
iRFP         IYRFASDFSGEVIAEDRCAEVESLGLHVPASTVPAQARRLYTINPVRIIPDINYPVPV 229
              : : * : * * : : * * : : * * * * * * * * : : * . . * *

ΔDrBphP      DPVLNPQTNAPTLGGAVLRATSPMHMQYLRNMGVGSSLSVSVVVGGQLWGLIACHHQTP 294
IFP1.4       DPVLNPQTNAPTLGGAVLRATSPMHMQYLRNMGVGSSLSVSVVVGGQLWGLIVCHHQTP 294
ΔBrBphP      QPRISPLNGRDLDMSLSCLRSMSPIHQYLQNMGVGATLVCSLMVSGRLWGLIACHHYEP 286
mIFP         QPRISPLNGRDLDMSLSCLRSMSPIHQYMDMGVGATLVCSLMVSGRLWGLIACHHYEP 286
ΔRpBphP      TPDLNPVTGRPIDLSFAILRSVSPVHLEMRNIGMHGTMSISILRGERLWGLIACHHRKP 289
iRFP         TPDLNPVTGRPIDLSFAILRSVSPVHLEMRNIGMHGTMSISILRGERLWGLIVCHHRP 289
              * : . * . . : . : * * : * * * : : * * : : * * . : * * * * * * *

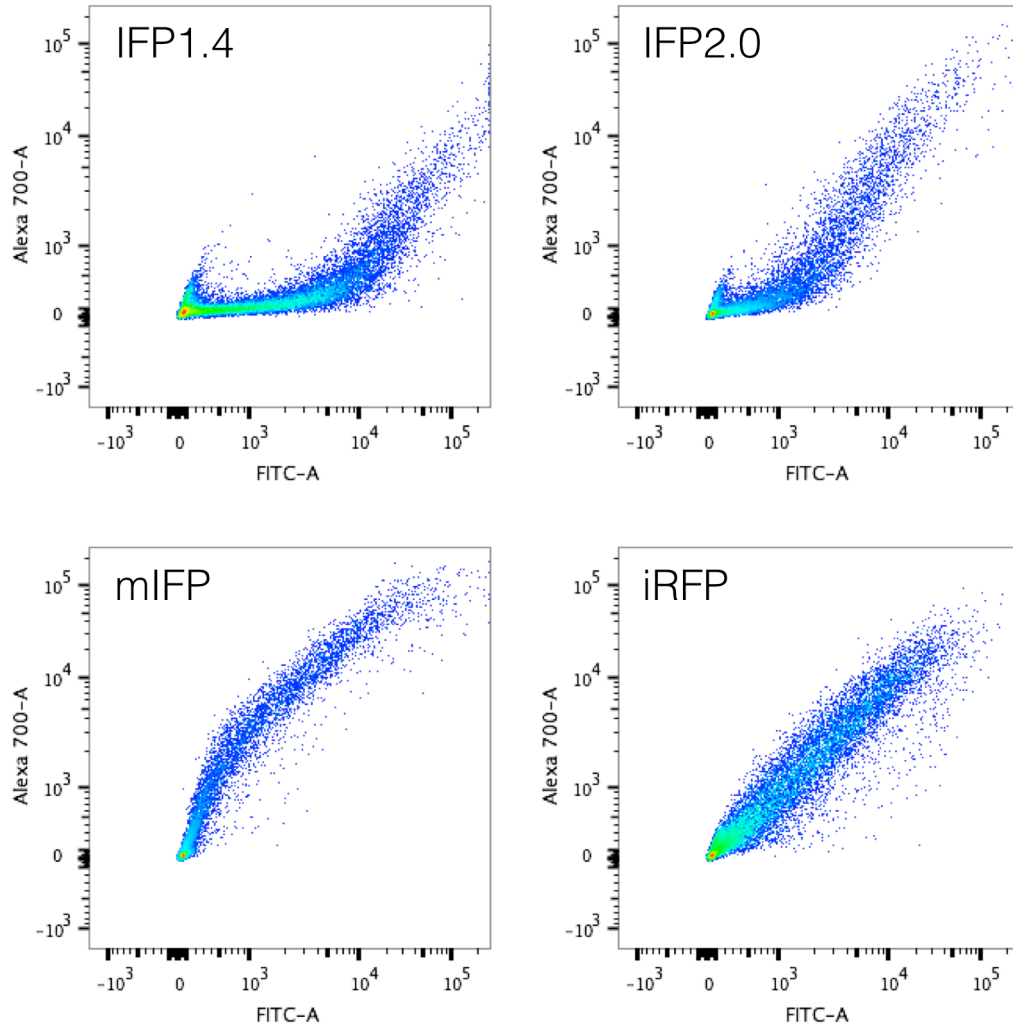
ΔDrBphP      YVLPPDLRTTLEYLGRLLSLQVQVKEA----- 321
IFP1.4       YVLPPDLRTTLEELGRKLSGQVQRKEA----- 321
ΔBrBphP      RFVPFDIRAAGEALAETCAIRIAALESFAQSQSE 315
mIFP         RFVPFDHIRAAGEALAETCAIRIATLESFAQSQSK 320
ΔRpBphP      NYVDLDGRQACELVAQVLAWQIGVMEE----- 316
iRFP         VYVDLDGRQACELVAQVLAWQIGVMEE----- 316
              : . * : * * . . : : : *

```

### Supplementary Figure 7.

Sequence alignment of engineered infrared fluorescent proteins and their parents.

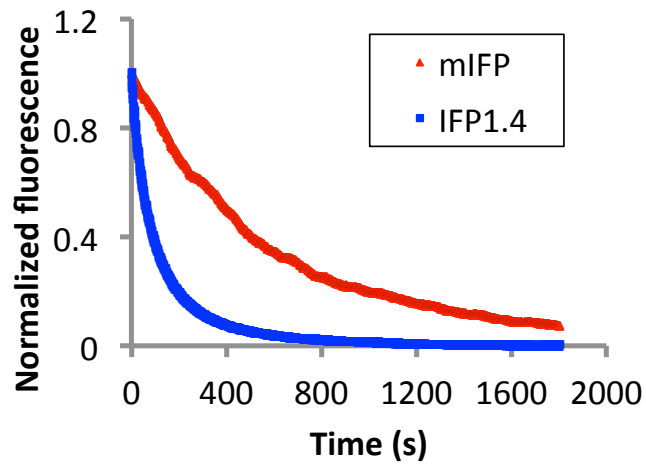
Mutations in IFP1.4 compared to its parent ΔDrBphP is shown in cyan; mutations in mIFP compared to its parent ΔBrBphP in yellow; mutations in iRFP compared to its parent ΔRpBphP2 in green.



### Supplementary Figure 8

Comparison of IFPs in cells by flow cytometer.

HeLa cells were transiently transfected with IFP1.4 IRES EGFP, IFP2.0 IRES EGFP, mIFP IRES EGFP or iRFP IRESEGFP. 48 hours after transfection, cells were then washed and suspended in 0.5mL PBS and analyzed on a flow cytometer. EGFP fluorescence was detected by the FITC-A channel (488 nm laser, 505/535 nm emission filter). IFP fluorescence was detected by the Alexa 700-A channel (640 nm laser, 708/753 nm emission filter). Data were processed using FlowJo software.

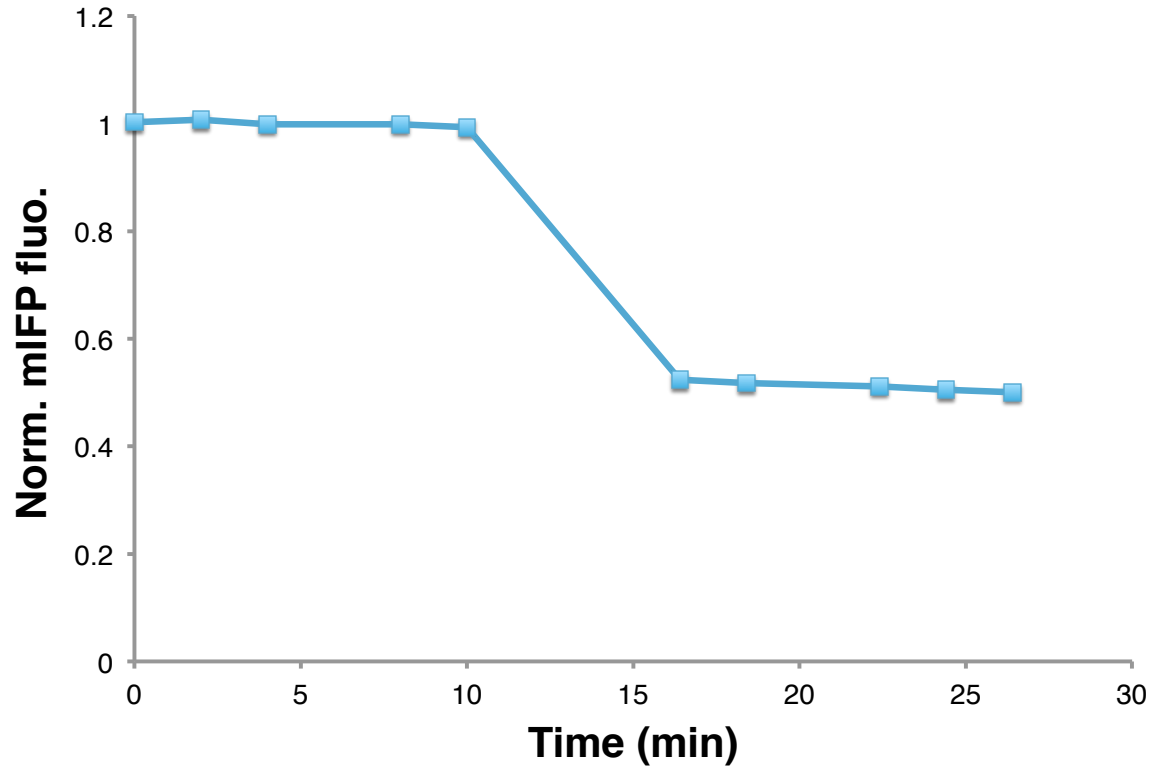


**Supplementary Figure 9.**

Photobleaching of mIFP and IFP1.4 in HEK293 cells.

Normalized fluorescence intensity over time under illumination of 100% 640 nm laser.

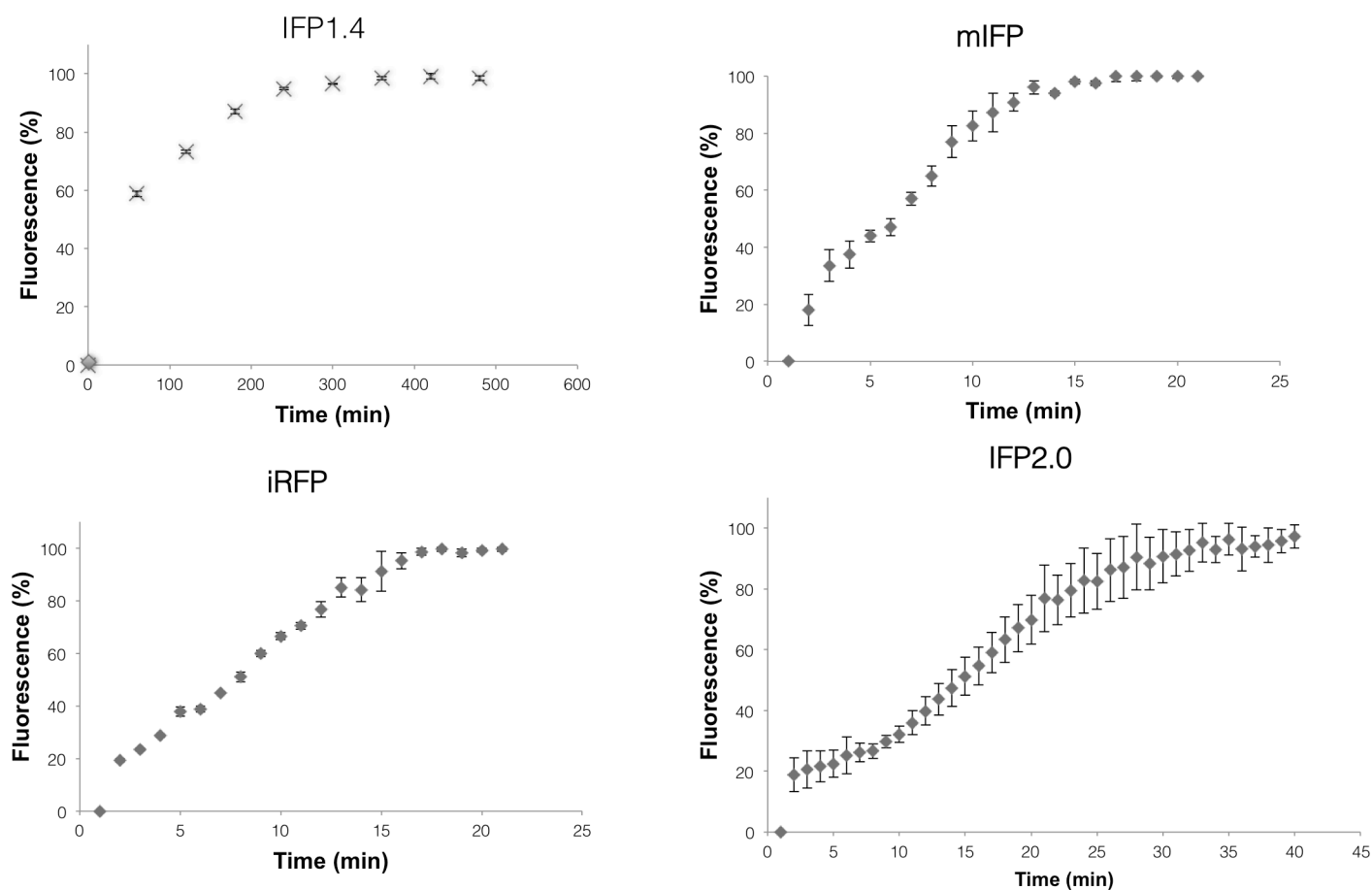
The laser power is 13.4 mW and illumination light intensity is 1.83 W/cm<sup>2</sup>.



**Supplementary Figure 10.**

Irreversible photobleaching of mIFP in HEK293 cells.

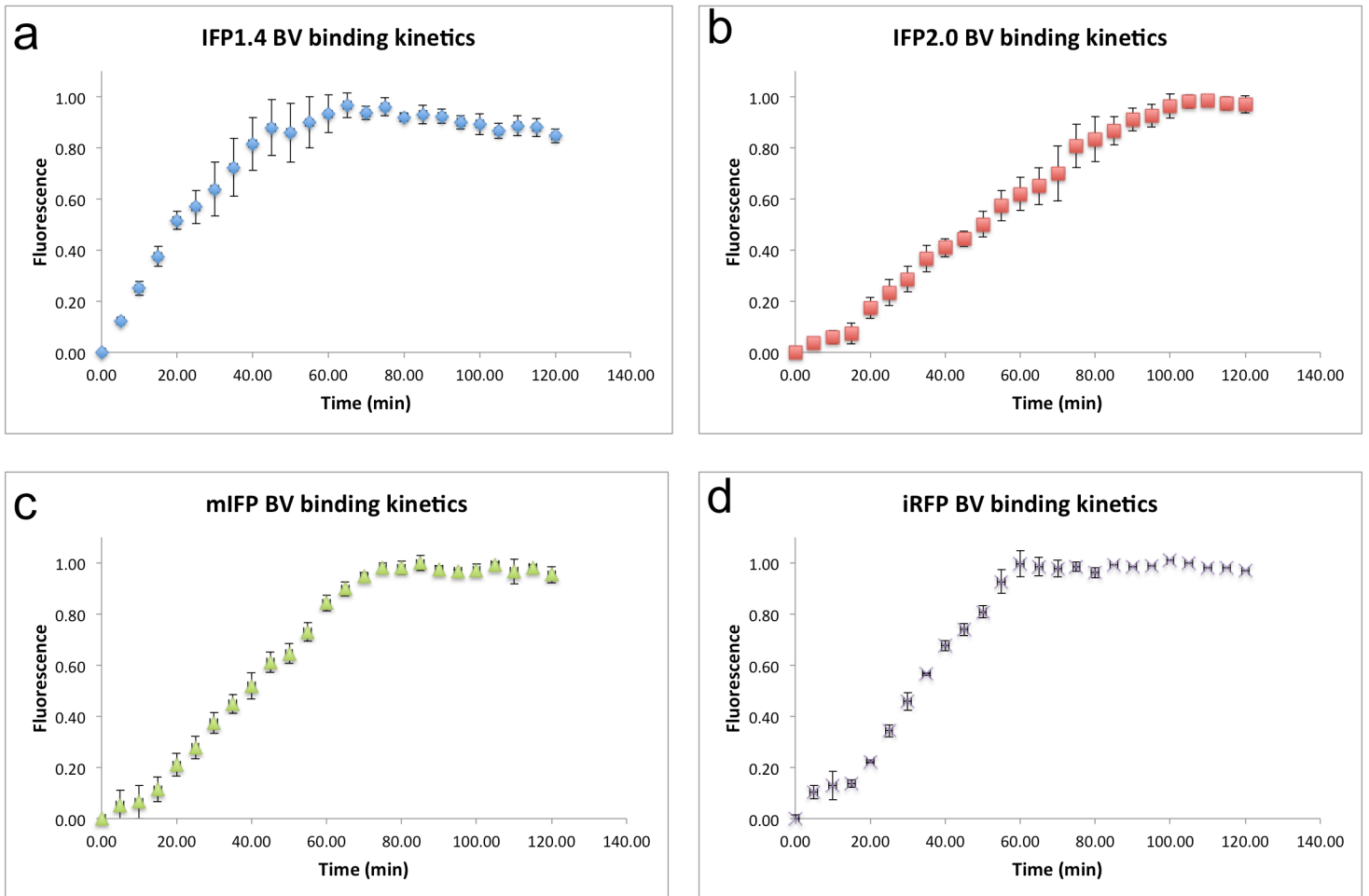
Fluorescence intensities were measured at 0, 2, 4, 8 and 10 min., followed by continuous illumination (from 10 to 16 min.) of 100% 640 nm laser that photobleaches mIFP about 50%. Following this photobleaching, fluorescence intensities were measured again at 16, 18, 22, 24, and 26 min.



### Supplementary Figure 11

Protein maturation rate in *E. coli*.

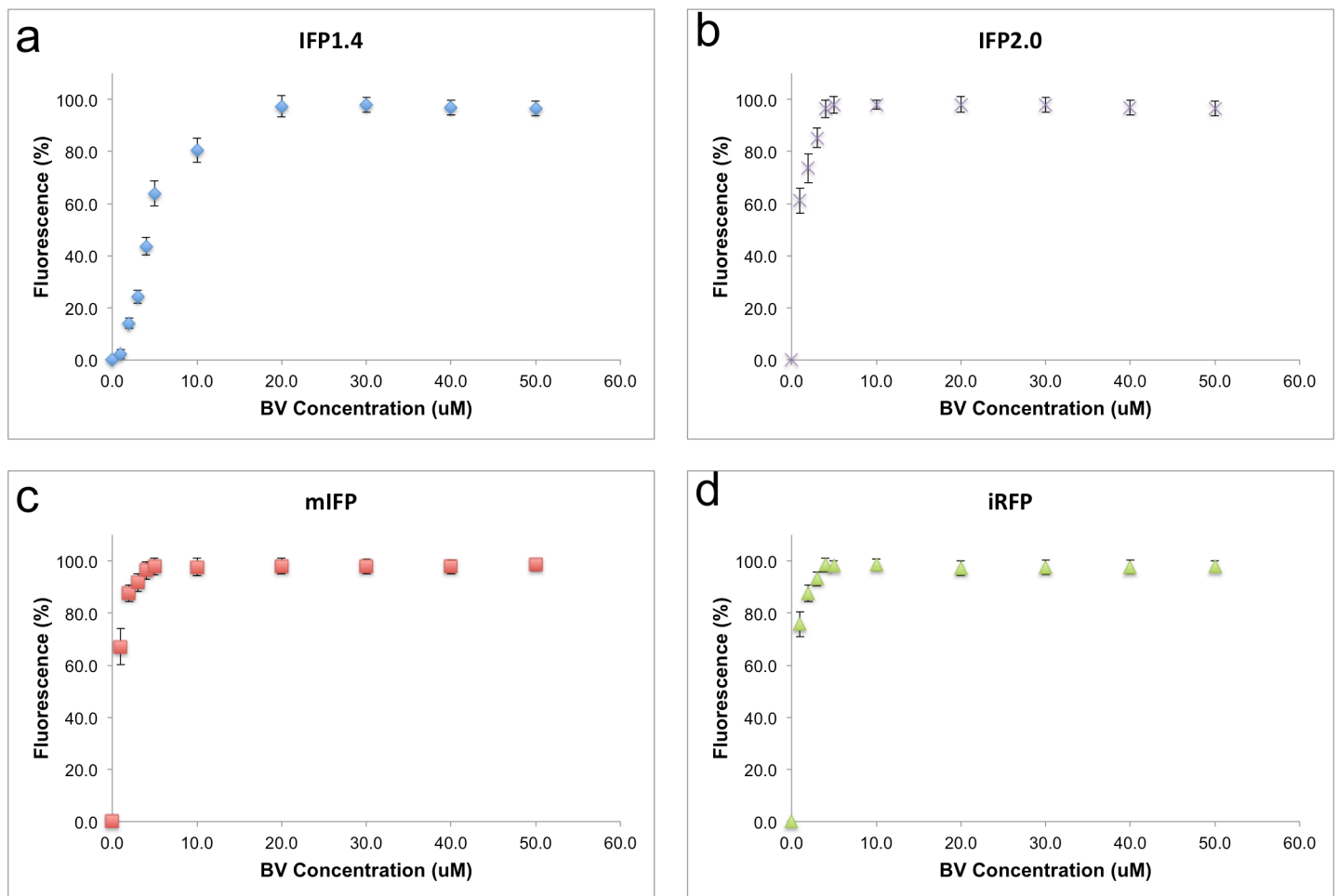
mIFP, IFP2.0 and iRFP mature slower compared to IFP1.4 in *E. coli* at 37 °C, with a maturation half-time  $4.6 \pm 0.9$  hrs (mIFP),  $8.7 \pm 0.6$  hrs (iRFP),  $19.6 \pm 7.5$  (IFP2.0) and  $0.88 \pm 0.02$  hr (IFP1.4). The standard deviation (std) is obtained from three independent experiments. Note that IFP1.4 data shows very small std.



### Supplementary Figure 12

BV binding kinetics.

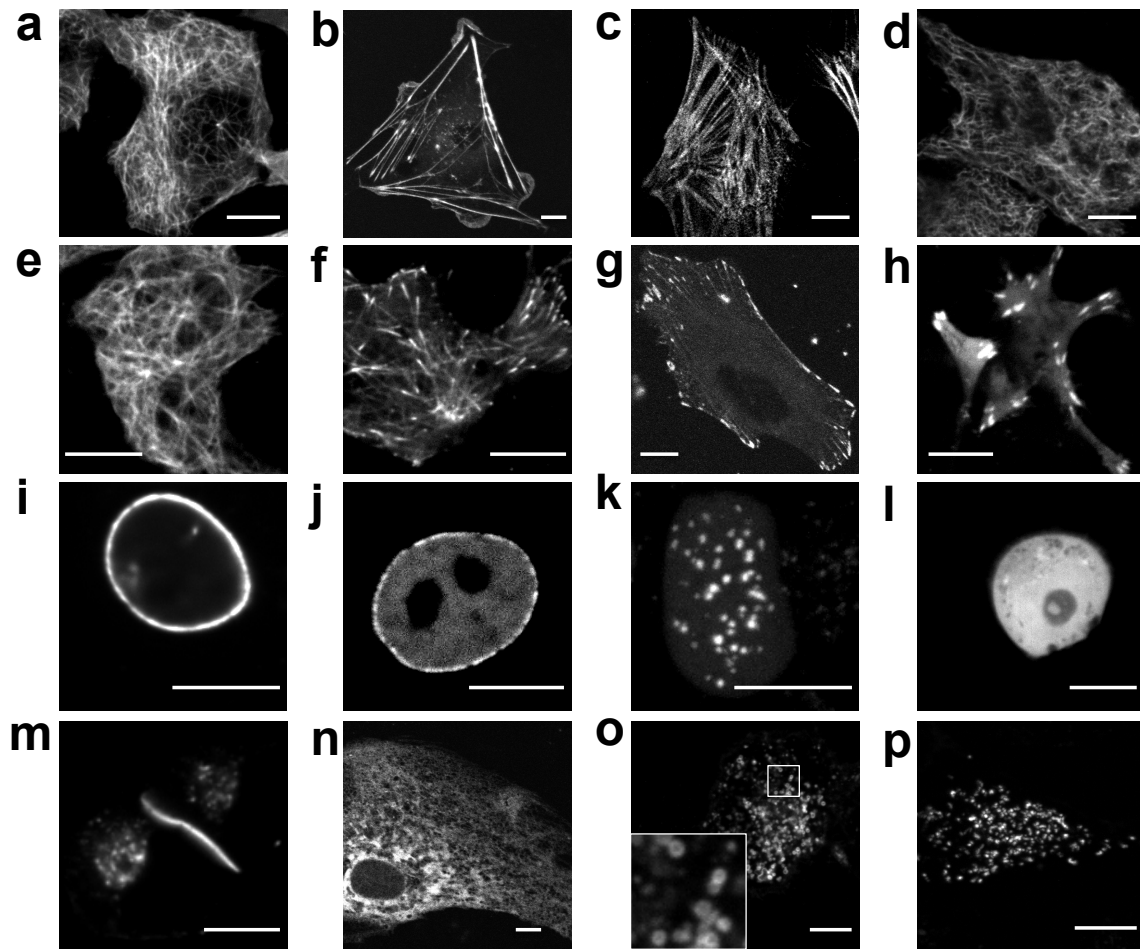
Live LN229 cells expressing IFPs (and IRES GFP) were treated with 25  $\mu$ M BV. The green and infrared fluorescence intensity was measured over time. The infrared fluorescence intensity (normalized by GFP) was plotted against time. BV binds to iRFP, IFP2.0 and mIFP at a slower rate than IFP1.4, with binding half-time  $51 \pm 9$  min. (mIFP),  $34 \pm 4$  min. (iRFP),  $102 \pm 15$  min. (IFP2.0), and  $17 \pm 2$  min. (IFP1.4). The standard deviation is obtained from three independent experiments.



### Supplementary Figure 13

Dependence of brightness of IFP-expressing cells on the BV concentration.

The brightness of live LN229 cells expressing IFPs (and IRES EGFP) is dependent on BV concentration. The BV binding curves could be fitted and processed by a Scatchard equation. The  $K_D$  of IFP1.4, IFP2.0, mIFP and iRFP were  $4.84 \pm 0.42$ ,  $0.83 \pm 0.02$ ,  $0.58 \pm 0.10$ ,  $0.49 \pm 0.05$ , respectively, suggesting that BV binds to mIFP, IFP2.0 and iRFP more favorable than IFP1.4. The standard deviation is obtained from three independent experiments.

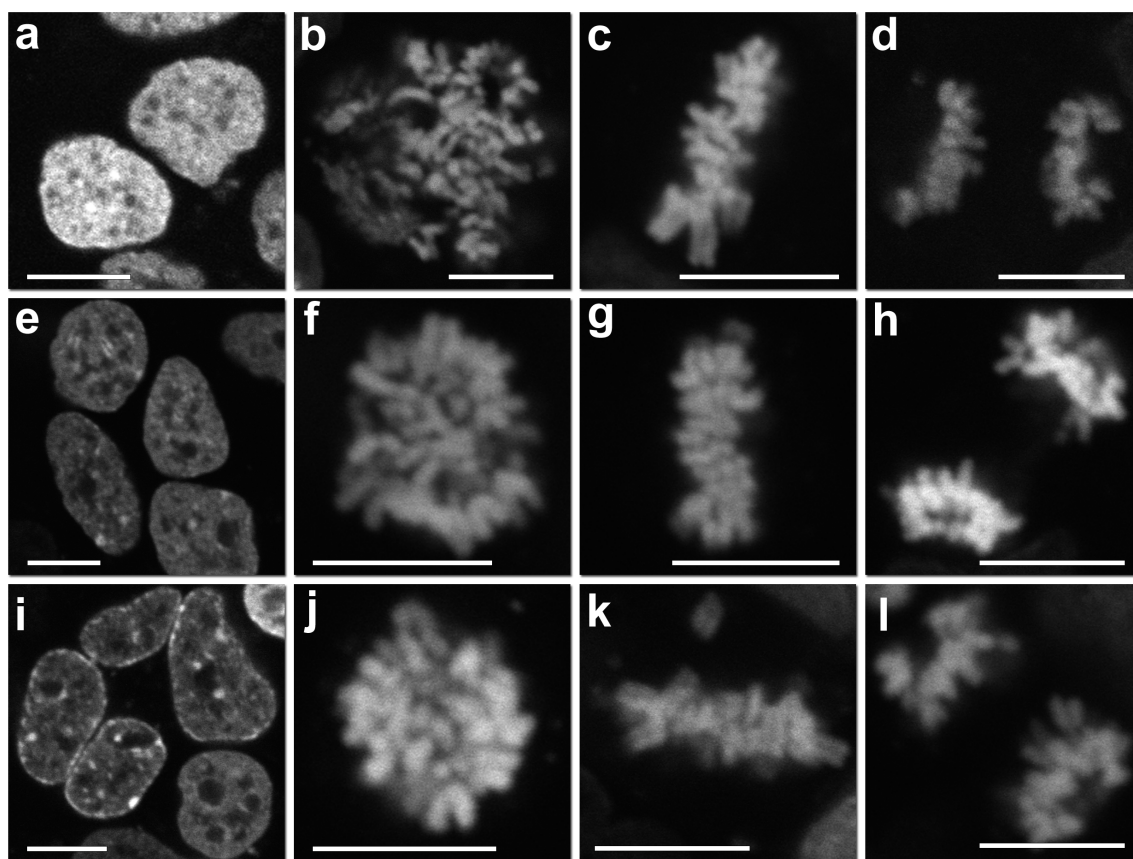


#### Supplementary Figure 14.

Fluorescence imaging of proteins fused to mIFP.

For each fusion, the N or C-terminal fusion and the linker amino acid length are indicated after the name of the targeted proteins: **(a-d)** Cytoskeletal proteins: **(a)** mIFP- $\alpha$ -tubulin-C-30 (human; microtubules); **(b)** mIFP- $\beta$ -actin-C-30 (human; actin cytoskeleton); **(c)** mIFP-Myotilin-C-26 (human; actin filaments); **(d)** mIFP-Keratin-N-17 (human; intermediate filaments; cytokeratin 18); **(e-f)** Cytoskeletal associated proteins: **(e)** mIFP-MAPTau-N-10 (human; microtubules); **(f)** mIFP-EB3-N-7 (human microtubule-

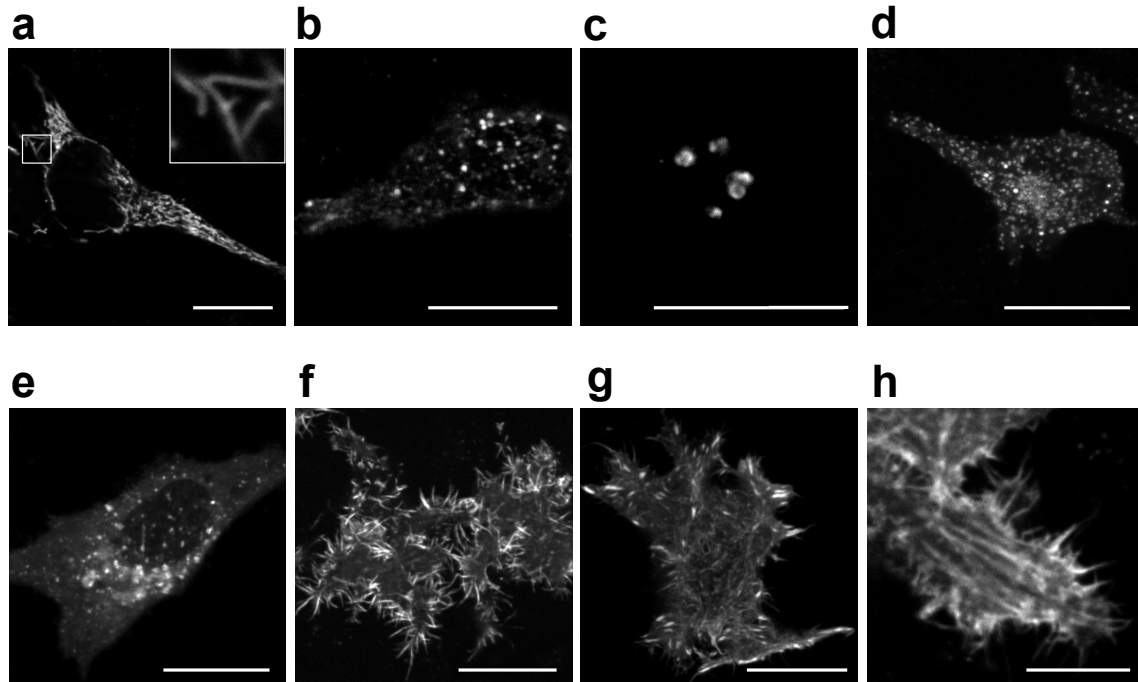
associated protein; RP/EB family); (**g-h**) Focal adhesion proteins: (**g**) mIFP-Zyxin-N-6 (human; focal adhesions); (**h**) mIFP-Vinculin-C-35 (human; focal adhesions); (**i-l**) Nuclear proteins: (**i**) mIFP-LaminA-C-30 (human; nuclear envelope); (**j**) mIFP-Nup50-N-10 (human; nuclear pore complex); (**k**) mIFP-CENPB-N-22 (human; centromeres); (**l**) mIFP-CAF1-C-22 (mouse; chromatin assembly factor); (**m**) Gap junction protein: mIFP-Cx43-N-7 (rat  $\alpha$ -1 connexin 43; gap junctions); (**n-p**) Intracellular organelles: (**n**) mIFP-Calnexin-N-14 (human; endoplasmic reticulum); (**o**) mIFP-LAMP1-N-20 (rat; lysosomal membrane glycoprotein 1; lysosomes); (**p**) mIFP-PMP-N-10 (human; peroxisomes). PtK2 cells (CCL-56; ATCC) were used in panel (**b**), HeLa CCL2 (ATCC) cells in the remaining panels. Scale bars represent 10  $\mu$ m. The cells were imaged at 60X magnification.



### Supplementary Figure 15

Fluorescence imaging of mIFP-Histone fusions.

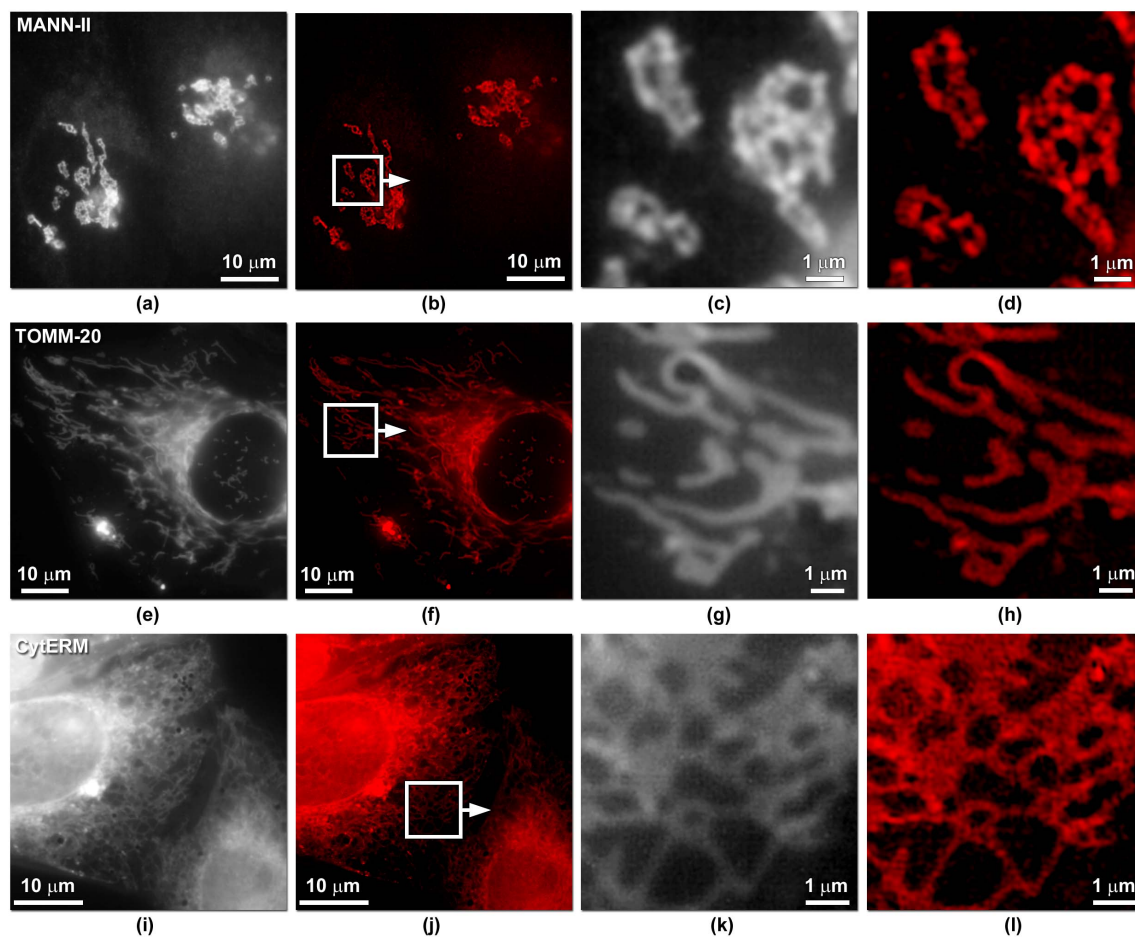
(a)-(d) mIFP-H1-N-10 (mouse) in HEK293 cells; (a) interphase; (b) prophase; (c) metaphase; (d) anaphase; (e)-(h) mIFP-H2B-C-10 (human) in HeLa S3 cells; (e) interphase; (f) prophase; (g) metaphase; (h) anaphase. (i)-(l) mIFP-H2B-C-10 (human) in HEK293 cells; (i) interphase; (j) prophase; (k) metaphase; (l) anaphase. Scale bars represent 10  $\mu\text{m}$ .



### Supplementary Figure 16.

Fluorescence imaging of proteins fused to mIFP.

Fluorescence imaging of mIFP fusion vectors. For each fusion, the N or C-terminal fusion and the linker amino acid length are indicated after the name of the targeted proteins: : (A) mIFP-TOMM20-N-10 (human translocase; mitochondria); (B) mIFP-Endosomes-C-26 (human; RhoB GTPase); (C) mIFP-Fibrillarin-C-19 (human; nucleoli); (D) mIFP-Clathrin-C-27 (human; light chain B); (E) mIFP-Rab4a-C-19 (human; endosomes); (F) mIFP-sEspin-C-30 (rat; actin bundling); (G) mIFP-LASP1-C-22 (human; actin binding); (H) mIFP-Lifeact-N-7 (yeast; actin). The cell line used for expression of the mIFP constructs was HeLa CCL2 (ATCC) cells. Scale bars represent 20  $\mu\text{m}$ .

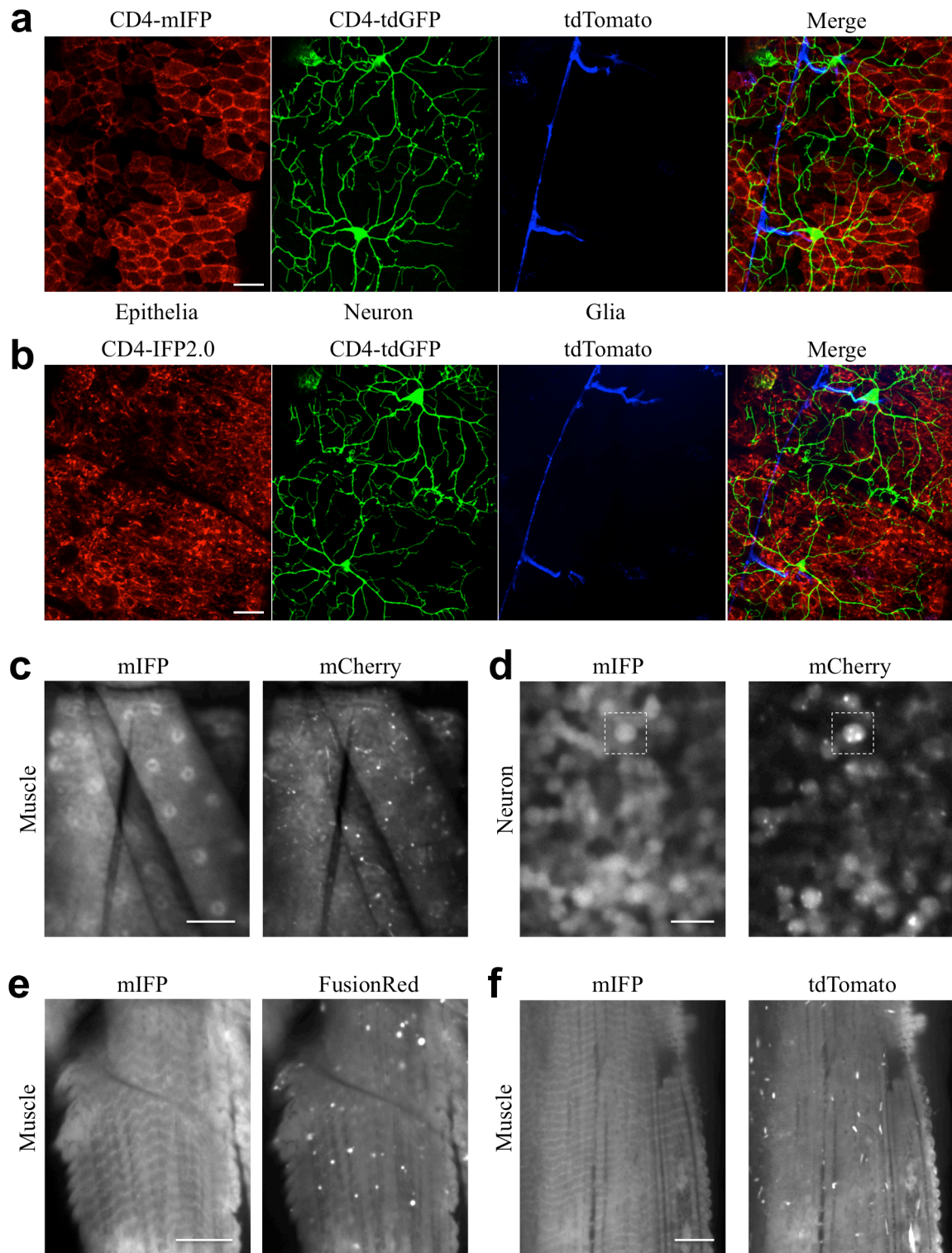


### Supplementary Figure 17.

Structured Illumination Microscopy (SIM) and respective widefield images.

MANNII (a-d), TOMM20 (e-h), and CytERM (i-l) fused to mIFP. All images are of HeLa cells fixed using 2% (w/v) paraformaldehyde and mounted in gelvatol. (a) Low magnification SIM and (b) widefield images of two cells expressing the golgi-labeling protein MANNII. The box in (b) denotes the zoomed region-of-interest (ROI) shown in (c,d). (c) Zoomed widefield image and (d) zoomed SIM image of the same area. (e) Low magnification SIM and (f) widefield images of a cell expressing the mitochondrial membrane protein TOMM20. (g) Zoomed widefield and (h) SIM images of the ROI in

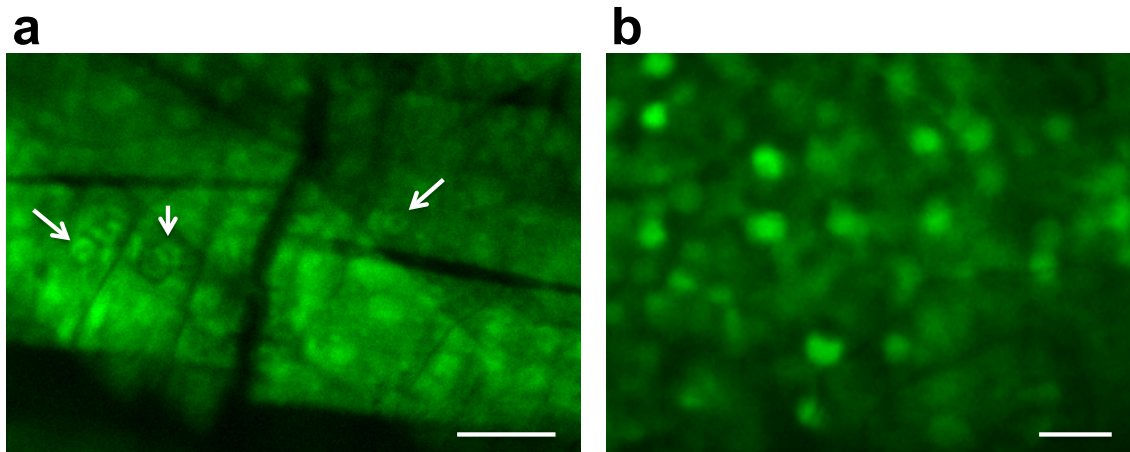
(f). Widefield (i) and SIM (j) image of a pair of cells expressing the endoplasmic reticulum transmembrane protein CytERM. Zoomed widefield (k) and SIM (l) images of the ROI in (j).



## Supplementary Figure 18

Comparison of mIFP to other FPs in *Drosophila*.

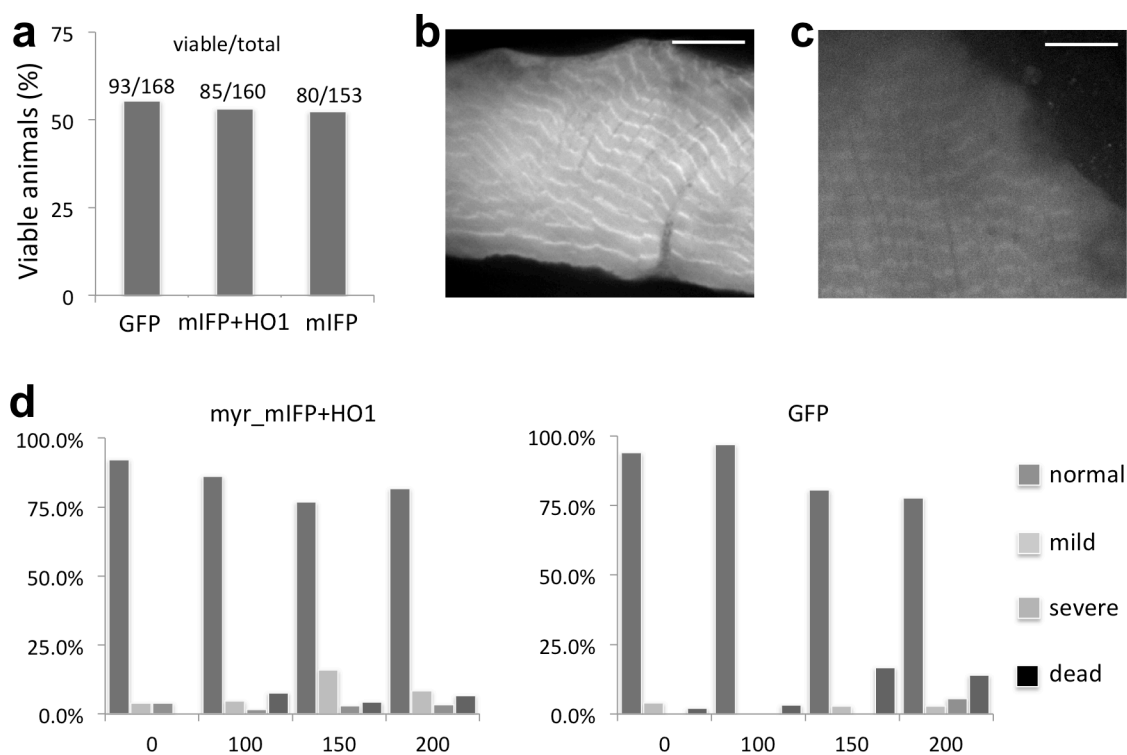
**(a, b)** Fluorescence images of epithelia, neurons and glia of second instar larvae expressing mIFP-CD4 T2A HO1 **(a)** or IFP2.0-CD4 T2A HO1 **(b)**, CD4-tdGFP and tdTomato, respectively. **(c)** Fluorescence images of the body muscle of first instar larvae co-expressing mIFP T2A HO1 and mCherry. **(d)** Fluorescence images of the neurons in cortical layer of the ventral nerve cord of first instar larvae co-expressing mIFP T2A HO1 and mCherry. **(e)** Fluorescence images of the leg muscle of adult co-expressing mIFP T2A HO1 and FusionRed. **(f)** Fluorescence images of the leg muscle of adult co-expressing mIFP T2A HO1 and tdTomato. T2A is a self cleaving peptide derived from foot-and-mouth virus. HO1 is heme oxygenase 1 that converts heme to biliverdin (cofactor of mIFP). Scale bar, 20  $\mu\text{m}$  **(a, b, c)**; 10  $\mu\text{m}$  **(d, e, f)**.



**Supplementary Figure 19.**

Expression of GFP in *Drosophila*.

Fluorescence images of GFP expressing muscle (**a**) and neurons (**b**) in the first instar larvae. Arrows points to nuclear structures in the multinucleated muscle (a). Scale bar, 20  $\mu\text{m}$  (**a**); 10  $\mu\text{m}$  (**b**).

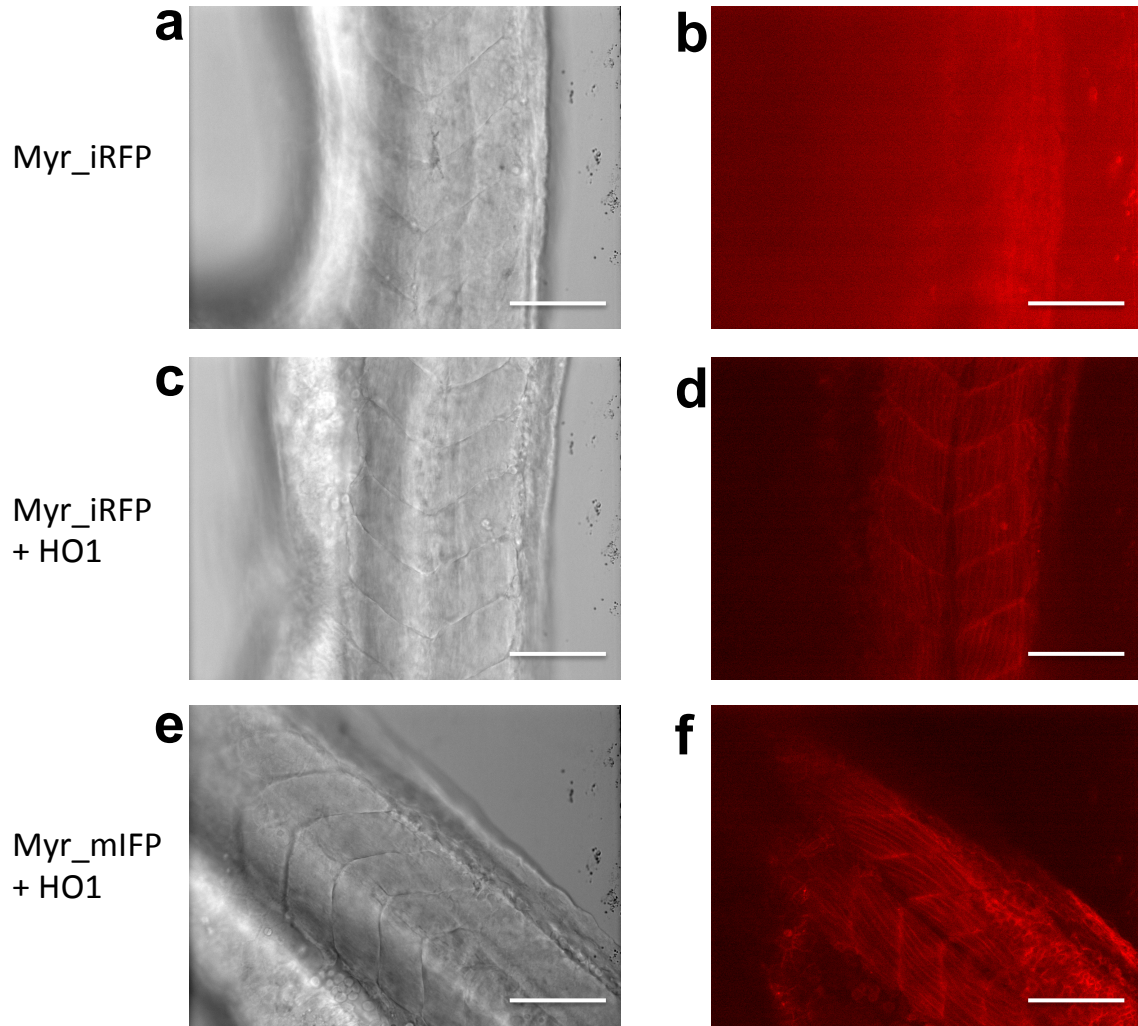


### Supplementary Figure 20

Toxicity assay of mIFP and the engineered cofactor biosynthesis.

**(a)** Viability assay of *Drosophila* ubiquitously expressing fluorophores at 25C driven by tubP-GAL4. The adult progeny were examined for reduced viability (% of animals carrying the fluorophore transgene relative to a balancer). The number of viable animals versus total animals is shown above the column. **(b)** Fluorescence image of mIFP with the engineered cofactor biosynthesis by co-expression of HO1, with 500 ms acquisition time. **(c)** Fluorescence image of mIFP with 5 seconds acquisition time. The fluorescence contrast was enhanced by 2 times in ImageJ. **(d)** Toxicity assay of zebrafish expressing fluorophores by RNA injection (pictogram). We examined at least 300 embryos for each construct. Embryos were scored as follows: normal to unaffected embryos were considered to have a wild-type phenotype (1<sup>st</sup> column); embryos with the presence of a

slightly curved tail and/or mild edema were considered mildly deformed (2<sup>nd</sup> column); embryos with smaller heads, major curves or a kink in the tail and/or severe edema were considered severely deformed (3<sup>rd</sup> column). Scale bar: 20  $\mu\text{m}$ .



**Supplementary Figure 21.**

Expression of iRFP with or without HO1 in zebrafish.

DIC and fluorescence images of zebrafish tail muscle expressing myristoylated iRFP (myr\_iRFP) (a, b), myr\_iRFP and HO1 (c, d), and myr\_mIFP and HO1 (e, f). Scale bar, 100  $\mu$ m. Fluorescence acquisition time: 4 seconds (b); 1 second (d, f).

**Supplementary Table 1.** Comparison of photophysical properties of bacteriophytochrome-derived infrared fluorescent proteins.

Protein	Absorbance maximum (nm)	Excitation maximum (nm)	Emission maximum (nm)	Extinction Coefficient based on protein concentration ( $M^{-1} cm^{-1}$ )	Extinction Coefficient based on absorbance ( $M^{-1} cm^{-1}$ )	Quantum yield (%)	Photostability $\tau_{1/2}$ (s)	Stoichiometry
mIFP	683	683	704	55,000	82,000	8.4	400*	Monomer <sup>&amp;</sup>
IFP1.4	685	683	705	53,000	88,000	7.3	64*	Monomer <sup>#</sup> (Weak dimer <sup>§</sup> )
IFP2.0	690	690	711	74,000	98,000	8.1	70*	Monomer <sup>#</sup> (Weak dimer <sup>§</sup> )
iRFP		690 <sup>2</sup>	713 <sup>2</sup>	60,000	89,000 (98,000 <sup>2</sup> )	6.9 (6.3 <sup>2</sup> )	1,520 <sup>2</sup> (>1800*)	Dimer
Wi-Phy <sup>1</sup>	701		719		93,000	4.7		Monomer <sup>#</sup>
iRFP670 <sup>2</sup>		643	670		114,000	11.1		Dimer
iRFP682 <sup>2</sup>		663	682		90,000	11.3		Dimer
iRFP702 <sup>2</sup>		673	702		93,000	8.2		Dimer
iRFP720 <sup>2</sup>		702	720		96,000	6.0		Dimer

\* Measured in live cells in this work.

<sup>&</sup> Monomer by size exclusion chromatography and analytical ultracentrifugation.

<sup>#</sup> Monomer by size exclusion chromatography.

<sup>§</sup> Weak dimer by analytical ultracentrifugation.

<sup>1</sup> Auldridge, M. E., Satyshur, K. A., Anstrom, D. M., & Forest, K. T. (2012). Structure-guided Engineering Enhances a Phytochrome-based Infrared Fluorescent Protein. *The Journal of Biological Chemistry*, 287(10), 7000–7009.

<sup>2</sup> Shcherbakova, D. M., & Verkhusha, V. V. (2013). Near-infrared fluorescent proteins for multicolor in vivo imaging. *Nature Methods*. doi:10.1038/nmeth.2521

**Supplementary Table 2. List of oligonucleotides used in this work**

Name	SEQUENCE (5' TO 3')
pB1	GGGCTAGAAATAATTTTGTTTAACTT
pB2HO	ATACCCATGAGTGTCAAC
mIFPM199T 1S	TTAAACTTAAGCTTG CCACCA TGC C
mIFPM199T 1AS	GAGCGATCTGGGGGATCGT
mIFPM199T 2S	ACGATCCCCCAGATCGCTC
mIFPM199T	GCAATACCGGAGTACTCGAGTCAC
mIFP hindIII S	AACTTAAGCTTGCCACCATGTCCGGTACCGCTG
mIFP XhoI AS	GAGTACTCGAGTTTGGACTGAGACTGTGC
mIFP EcoRV S	GCCCTCGATATCTTTGGACTGAGACTGTGC
mIFPH2B 1AS	GCCTCCGGAGCCTCCAGATCTGAGTCCGGATTTGGACTGAGACTGTG
mIFPH2B 2S	AAACTTAAGCTTGCCACC
mIFPH2B 2AS	GAGTACTCGAGTTACTTAGCGCTGGTGT
iRFP hindIII	CTTAAGCTTGCCACCATGGCGGAAGGATCC
iRFP1AS	GCTCCGACGGCCGCGCCAGGCTCGGCCAAGGCG
iRFP2S	CGCCTTGCCGAGCCTGGCGCGGCCGTCGGAGC
iRFP2AS	CCCGCTGGGGAGGCTCCAATTCCAGGAAGATGAGCTGA
iRFP3S	TCAGCTCATCTTCTGGAATTGGAGCCTCCCCAGCGGG
iRFP3 XhoI AS	AGTACTCGAGTCACTCTTCCATCACGCC
CD4-mIFP S BamH1	AGGCGGATCCTCGGTACCGCTGACTACC
CD4-mIFP AS XbaI	TAATTCTAGATTATTTGGACTGAGACTGTGCAA
CD4-iRFP S BamH1	AGGCGGATCCATGGCTGAAGGCTCAGTCGCCAGGCAGC
CD4-iRFP AS xbaI	TAATTCTAGATTACTCTTCCATCACGCC
mIFP12-AgeI-C-f	GCGCTACCGGTCGCCACCATGTCCGGTACCGCTGACTACCTCAGCATTCCGG
mIFP12-BspEI-C-r	TCTGAGTCCGGAACCTTCGCCACCGCTTCCGCCCGCGCTTCCGCCACCTTT GGACTGAGACTGTGCAAAGCTCTCCAGCGTC

**Supplementary Video 1. Z-section confocal imaging of mIFP- $\alpha$ -tubulin in live cells.**

HEK293 cells transiently transfected with the fusion construct were imaged with z-section (step size 1  $\mu\text{m}$ ). The entire field of view is shown.

**Supplementary Video 2. Time lapse imaging of mIFP- $\alpha$ -tubulin in live cells.**

HEK293 cells transiently transfected with the fusion construct were imaged every 15 min. The entire field of view is shown.

**Supplementary Video 3. Time lapse imaging of mIFP- $\beta$ -actin in live cells.**

Ptk2 cells transiently transfected with the fusion construct were imaged every 3 min.

**Supplementary Video 4. Time lapse imaging of mIFP-EB3 in live cells.**

HeLa cells transiently transfected with the fusion construct were imaged every 2 seconds.

**Supplementary Video 5. Time lapse imaging of mIFP-H1 in live cells.**

HeLa cells transiently transfected with the fusion construct were imaged every 2 min.

**Supplementary Video 6. Z-section two-color confocal imaging.**

HEK293 cells transiently transfected with the mRuby-H2B (in yellow) and mIFP- $\alpha$ -tubulin (in red) were imaged with z-section (step size 1  $\mu\text{m}$ ).

**Supplementary Video 7. Time lapse imaging of CD8-GFP in Drosophila.**

Entire *Drosophila* embryo expressing UAS-CD8-GFP driven by elav-GAL4 was imaged every 10 min, which revealed the ventral nerve cord condensation.

**Supplementary Video 8. Time lapse imaging of mIFP-H3.3 T2A HO1 and CD8-GFP in *Drosophila*.**

Entire *Drosophila* embryo expressing UAS-mIFP-H3.3 T2A HO1 (in red) and UAS-CD8-GFP (in green) driven by elav-GAL4 was imaged every 10 min, which revealed the ventral nerve cord condensation.